Nature versus Nurture: Preservation and Destruction of Archean Cratons

H. Bedle[1], C.M. Cooper[2], and C.D. Frost[3]

[1]*School of Geosciences, University of Oklahoma, 100 East Boyd Street, RM 710, Norman, Oklahoma 73019, USA*

[2]*School of the Environment, Washington State University, PO Box 642812, Pullman, WA 99164, USA*

[3]*Department of Geology and Geophysics, University of Wyoming, Laramie WY 82071, USA*

Corresponding author: Heather Bedle (hbedle@ou.edu)

Key Points:

- The survival of Archean cratons depends both upon their *nature*—the initial conditions of formation—and *nurture*—the subsequent tectonic processes that may modify and destabilize cratonic lithosphere.
- Some cratons have survived by avoiding or being shielded from destabilizing tectonic processes. Metasomatism is particularly destructive because it affects buoyancy, viscosity, and integrated yield strength.
- Stability regime diagrams integrate both time and the magnitude of modification, and indicate that marginally stable cratons today may pass into conditions of marginal instability in the future, when even mild deformational stresses could trigger destruction.

Abstract

The factors that promote stability of Archean cratons are investigated from a combined geodynamic, geological, and geophysical perspective in order to evaluate the relative importance of *nature*—the initial conditions of a craton—versus *nurture*—the subsequent tectonic processes that may modify and destabilize cratonic lithosphere. We use stability regime diagrams to understand the factors that contribute to the intrinsic strength of a craton: buoyancy, viscosity, and relative integrated yield strength. Cratons formed early in Earth history when thermal conditions enhanced extraction of large melt fractions and early cratonization (cessation of penetrative deformation, magmatism and metamorphism) promote formation of stable Archean cratonic lithosphere. Subsequent processes that may modify and weaken cratonic lithosphere include subduction and slab rollback, rifting, and mantle plumes –processes that introduce heat, fluids, and partial melts that warm and metasomatize the lithosphere. We examine tomographic data from eight cratons, including four that are thought to be stable and four that have been proposed to be modified or destroyed. Our review suggests that continental lithosphere formed and cratonized prior to the end of the Archean has the potential to withstand subsequent deformation, heat, and metasomatism. Survivability is enhanced when cratons avoid subsequent tectonic processes, particularly subduction. It also depends on the extent and geometry of modification. However, because craton stability decreases as the Earth cools, marginally stable cratons that undergo even modest modification may be set on a path to destruction. Therefore, preservation of Archean cratons depends both on nature and nurture.

Plain Language Summary

Because of Earth's dynamic tectonic processes, much of its continental crust has been eroded and recycled and only a fraction of crust older than 2.5 billion years has survived to the present-day. These areas of old crust, known as Archean cratons, have not experienced deformation or magmatism for a billion years or more. This paper investigates whether craton survival is related to their *nature*, that is, the conditions of their formation, or to *nurture*, the subsequent events they experienced. Eight case studies are used to evaluate the properties and processes that promote craton stability. Nature is important: surviving Archean cratons tend to be buoyant, viscous, cold and thick. Some survive because they have not experienced destabilizing geologic processes that introduce heat, magma, and fluids. Others have been modified to various extents by these processes. Some have been weakened and thinned and other, only marginally

stable cratons are susceptible to future deformation and destruction. We conclude that both nature and nurture are essential to the survival of Earth's oldest crust.

1 Introduction

Initially studied from the surface of the Earth, cratons are large regions of stable continental crust that have undergone minimal deformation since Precambrian time. Whereas cratons were originally believed to be enduring features of the lithosphere, recent studies have revealed that some Archean cratons are susceptible to the tectonic forces that shape the planet and have been modified by subsequent events (e.g. Hu et al., 2018; Kusky et al., 2014; Liu et al., 2018; Snyder et al., 2017). Why are some regions prone to deformation whereas others maintain stability? Is this susceptibility to deformation linked to characteristics primed by their formation, in other words, is it a function of their "nature"? Or is it driven by exposure to subsequent dynamic conditions, which can be thought of as processes that "nurture"? Or is it a combination of the two? Improved understanding of the controls on modification of Archean lithosphere since the Precambrian will advance our knowledge of craton stability, crust-mantle interactions, and recycling of cratonic lithosphere.

To understand the preservation and destruction of Archean cratons, we present a geodynamic framework for evaluating craton stability whereby the intrinsic strength of a craton is proposed to be controlled by factors including buoyancy, viscosity, integrated yield strength, and whether or not the craton is surrounded by weaker material. We introduce stability regime diagrams as a means of conceptualizing the geodynamic controls on craton stability and the drivers that may destabilize a once-stable region. We use this conceptualization to frame the nature versus nurture argument as well as to contextualize the tectonic and geologic processes that may promote craton destruction.

Next we examine eight case studies: four cratons that appear to have survived to the present-day unaffected by later tectonic processes: Pilbara, Yilgarn, Zimbabwe and Kaapvaal, and four cratons that may have had part or all of their cratonic mantle lithosphere modified or destroyed: Wyoming, North China, Amazonia, and Madagascar cratons. We frame our synthesis by exploring the influence of a craton's properties established during formation versus subsequent tectonic events experienced in its geologic history on its (in)stability to discern whether some cratons were more susceptible to deformation from their onset or require post-formation modification. We generalize from these examples our conclusion that cratons are created with variable stability. However, no craton is immune to modification given exposure to destabilizing tectonic processes and the gradual decrease in stability related to slow cooling of the planet. Craton survival is maximized through armoring by younger orogens and avoiding exposure to tectonic processes that destroy cratonic lithosphere.

2 What is a craton?

2.1 Geological properties of cratons

Geologically, cratons are defined as tectonically quiescent, long-lived stable continental regions. The origin of the word “craton,” as summarized by Şengör (1999), came from “kratogen,” a term coined by Kober (1921) to denote areas that are “born strong,” in contrast to orogens. They are regions that have not experienced the penetrative deformation, calc-alkalic magmatism and metamorphism that characterizes orogenic belts. Cratons may experience “cratogenic deformation,” that is, “non-penetrative deformation creating blocky structures with low to medium strain, commonly with no metamorphism and only sparse alkalic magmatism” (Şengör, 1999, quoting Stille, 1940)). Many cratons are Archean in age (Fig. 1). They are characterized by low surface heat flow (Nyblade & Pollack, 1993), which reflects the colder and thicker lithosphere than is associated with orogenic belts.

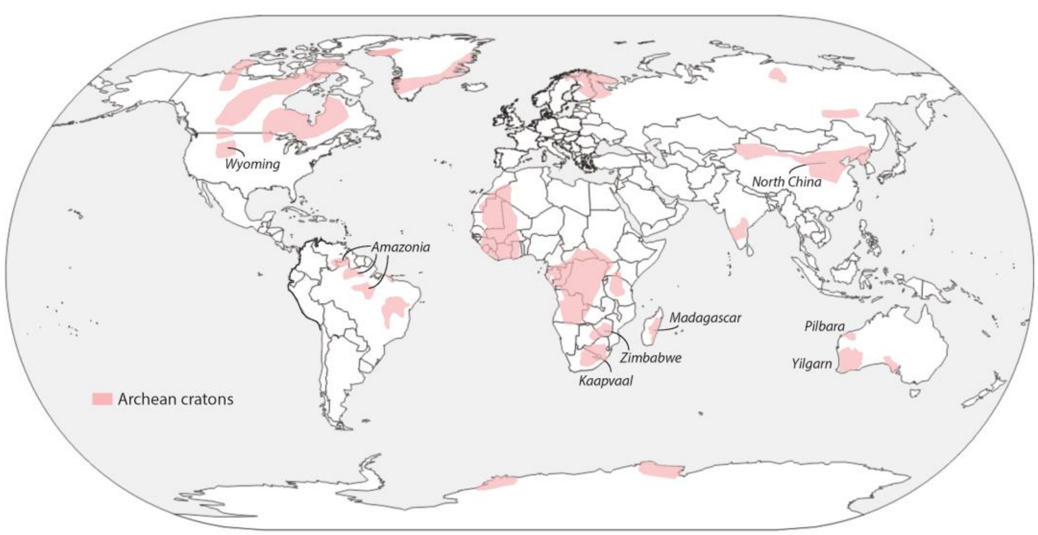

Figure 1. Archean cratons (> 2.5 Ga) are found on all continents. Cratons examined as case studies are labeled.

Cratonic keels are defined by relatively cold and thick lithosphere, which can be studied using geochemical and geophysical techniques. The keels of Archean craton may extend to depths of 200-300 km, as defined by the depth of the sub-continental lithospheric mantle (Prodehl & Mooney, 2012). Jordan (1975, 1988) suggested that the negative thermal buoyancy associated with the old and cold lithosphere is exactly offset by a positive chemical buoyancy leaving cratonic lithosphere neutrally buoyant, a concept known as the "isopycnic hypothesis". Information about the composition of this lithosphere is available from the study of subcratonic mantle xenoliths. These tend to have depleted compositions consistent with the removal of high degrees of partial melt and water. The Mg/(Mg+ Fe)-enriched and Ca and Al-depleted residual lithospheric mantle is less dense and more buoyant than the fertile mantle (Jordan, 1979; Lee et al., 2005). The extraction of partial melt depletes the mantle of water and in heat-producing elements, leaving it cold, strong, and viscous relative to the surrounding mantle lithosphere (Pollack, 1986).

The age of subcontinental mantle xenoliths generally corresponds to the age of the overlying crust (Carlson et al., 2005), indicating that the subcontinental lithospheric mantle is mechanically coupled to the crust and serves as a long-lived, viscous and buoyant cratonic keel. There is some evidence to suggest that the older the crust, the higher the degree of melt depletion from the underlying mantle lithosphere, which in turn suggests that the older the craton, the greater the compositional buoyancy of its mantle lithosphere, thickness, and overall strength and survivability of the craton (Poudjom Djomani et al., 2001).

2.2 Geodynamical properties of cratons

Geodynamical studies have demonstrated that craton stability is controlled by the intrinsic strength of the cratonic lithosphere and/or by being surrounded by weaker material (Cooper & Conrad, 2009; Lenardic et al., 2000; McKenzie et al., 2015). Intrinsic strength may be controlled by its buoyancy and viscosity (e.g., Lenardic and Moresi, 1999; Wang et al., 2014) and integrated yield strength (e.g., (Cooper et al., 2006).

As described above, the lithospheric mantle of cratons is proposed to have enhanced buoyancy and viscosity driven by dehydration and melt depletion occurring during formation (e.g., Carlson et al., 2005). The enhanced buoyancy was proposed by Jordan (1975, 1988) to explain stability of thick, old, and cold cratonic lithosphere. Yet buoyancy alone cannot provide stability and longevity: if not sufficiently viscous, buoyant lithosphere can viscously relax, pancake out, dome, or become entrained within mantle flow (Lenardic & Moresi, 1999); indeed, models focusing primarily on the role of buoyancy in stability of lithosphere demonstrate that that cratonic lithosphere is marginally stable (Cottrell et al., 2004). Higher values of viscosity can suppress deformation occurring along the margin (Lenardic & Moresi, 1999; Currie & van Wijk, 2016) as well as dripping at the base (Conrad & Molnar, 1999). The integrated yield strength of the cratonic lithosphere adds an additional component to stability by supplying the means to resist brittle failure, shearing, and plastic yielding (Lenardic et al., 2003; Cooper et al., 2006). The integrated yield stress is determined by the effective friction coefficient and cohesion as well as the thickness of the lithosphere (Byerlee, 1968), and thus craton stability is dependent upon depth of the cratonic keel.

The intrinsic strength provided by the combination of enhanced buoyancy, viscosity, and integrated yield stress of the cratonic lithosphere sets the conditions for stability as well as longevity. Stability implies that the cratonic lithosphere resists deformation within a particular tectonic setting. Longevity, rather, demonstrates the craton's ability to resist deformation, or remain stable, during evolving tectonic settings. In other words, cratons must not only stabilize shortly after formation, but also remain stable over the range of their lifetime. Yet, convective stresses at depth, and those that drive surface tectonics, do not remain constant as the Earth ages, but increase as the Earth continues to cool (Sandu et al., 2011). Thus, a craton originating with strong lithospheric material will be best able to withstand the progressive increase in stress and potential for deformation (Cooper et al., 2006; Beall et al., 2018). However, this requirement poses challenges in explaining craton formation as the forces required to thicken initially strong material may not be sufficient during the early Earth (Cooper et al., 2006; Beall et al., 2018).

If, however, proximity to weaker material is the stronger control on craton stability, then the conditions for longevity may be relaxed as the cratonic lithosphere itself is protected by surrounding material. The weaker material acts as a buffer zone around the margins focusing deformation away from the cratonic interior (Lenardic et al., 2000; Yoshida, 2012); cratonic lithosphere does not need to be uniquely strong, just stronger than the surrounding lithosphere. Thus, during times of accretion, continental collision or rifting, deformation is initiated in the weak margins (e.g., Wenker & Beaumont, 2018a). This scenario could explain the role of cratons in Wilson cycles (McKenzie et al., 2015) or continental collision (Yoshida, 2010) by focusing deformation in mobile/orogenic belts. In addition, weaker material at the base of cratonic lithosphere can also act as a buffer zone, safeguarding against shearing along the bottom of the craton driven by interacting with the convecting mantle (Cooper & Conrad, 2009).

2.3 Geophysical properties of cratons

Seismic imaging indicating a thick lithospheric keel is the defining geophysical feature of a stable Archean craton. Because geophysical methods reveal the present-day structure of the Earth's interior they must be used in combination with geologic data to infer the history of an area. Geophysical methods aim to identify the lithosphere-asthenosphere boundary (LAB), as well as the structure of the subcontinental lithospheric mantle. The LAB defines the limit between the Earth's outer thermal boundary layer and the weaker convecting layer below (Sleep, 2005). As such, the LAB is often used to define the base of cratonic keels. Identification of the LAB depends upon the geophysical method being deployed and can vary depending on the resolution and sensitivity of the particular method and data, and moreover the LAB is likely a diffuse boundary (Eaton et al., 2009; Fischer et al., 2010).

Seismic tomography has the capability to create regional- to global- scale velocity models that aid in the understanding of the geophysical characteristics of the lithosphere and the depth of the LAB and thus, the structure and subsurface extent of cratonic keels. 3D velocity models map both P- and S-wave velocity anomalies beneath the surface. The mapped seismic anomalies can then be interpreted in terms of the Earth's thermal and compositional structure, based upon how thermal and compositional variations perturb the seismic velocity. Thermal variations are known to alter the physical properties of the rock, such that warmer temperatures result in a slowing of Vp and Vs, and conversely, cooler temperatures result in an increase in the velocities. S-velocity is susceptible to the presence of fluids and will be lowered should fluids be present (Karato, 1995). Changes in chemical composition and mantle mineralogy will also result in velocity anomalies. In the upper mantle, variations in proportions of the main mantle minerals olivine, orthopyroxene, clinopyroxene, and garnet will alter the seismic velocities, both Vp and Vs. For example, an increase in clinopyroxene compared to olivine will lower Vs, a greater presence of garnet will increase Vs, and an increase in orthopyroxene as compared to clinopyroxene will increase Vs (Duffy & Anderson, 1989; Li et al., 2004). These relationships between seismic velocities and the thermal and compositional character of the mantle allow for insights into the current state of the cratons. Parameterization and algorithms used in each tomographic method result in variations between models, including variations in the depth and strength of the faster velocities that characterize the cratonic keels. Regardless of the specific models, these cratonic keels tend to display seismically fast velocity anomalies globally in Archean cratons that have not undergone modification since formation.

Geophysical techniques can also provide information about mid-lithospheric discontinuities (MLDs), which appear to be common structures within subcontinental lithospheric mantle (Abt et al., 2010; Fischer et al., 2010; Cooper et al., 2017). Current studies suggest that MLDs are ubiquitous to cratonic lithosphere. Possible origins include a solidified layer of volatile-rich melt, remnant subducting slabs, and compositional layering (Hopper & Fischer, 2015). Though they have been linked both to craton formation (Cooper & Miller, 2014) and craton modification (Selway et al., 2015), the presence of MLD in themselves is insufficient to delineate between craton stability or modification.

3 Evidence for stability

3.1 Geological evidence of craton stability

Rocks exposed at the surface and subsurface xenoliths are the two main sources of information that could provide evidence of the stability of cratons over geologic time. The geologic information can come from volcanic and sedimentary rocks deposited on the surface, igneous and metamorphic rocks formed at depth and subsequently exposed at the surface, and xenoliths from the lower crust and mantle brought to the surface in diatremes. However, this record is incomplete, particularly for the Archean. One reason is the limited exposure of Archean rocks in many cratons. For example, much of the Greenland portion of the North Atlantic craton is covered by ice, large areas of the Amazonian craton are under rainforest, and much of the Canadian shield is covered by younger sedimentary rocks. In the Wyoming craton, Archean rocks are exposed only in the cores of Laramide uplifts. On the other hand, some cratons, such as the Pilbara and Kaapvaal cratons, are relatively well-exposed and well-studied.

Moreover, it cannot be assumed that the Archean crust available for study today is representative of the crust that was formed. The Archean history of a craton may be overprinted by later orogenic events that obscure the earlier record. Some areas or compositions of Archean crust may be more likely to be preserved, and others susceptible to being recycled, either by sedimentary processes or by assimilation by younger magmas. Likewise, xenoliths are sparse and sample the subsurface incompletely. Studies of the age and geochemical characteristics of detrital and inherited zircon provide some information about rocks that are no longer present for direct examination and petrogenetic studies of younger igneous rocks help identify the character of magma source rocks at depth.

Despite these limits on our understanding of Archean cratons, there are geologic characteristics that may identify cratons with strong, buoyant, and thick cratonic lithosphere (Table 1). The first is the time of craton formation. Cratonic mantle lithosphere that formed early in Earth history when ambient mantle potential temperature was greatest may have undergone greater degrees of melt depletion and therefore have greater compositional buoyancy and strength. Herzberg & Rudnick (2012) argue that mantle temperature may have peaked at between 3.5 and 2.5 Ga, based on models of Earth's thermal history by Korenga (2008), and thus the most depleted mantle residues formed during the Archean.

Table 1
Characteristics of strong, long-lived cratons

Geodynamical	**Geological**	**Geophysical**
Buoyant, thick lithosphere	Early-formed crust, high melt fraction leaves buoyant residual mantle lithosphere	Deep lithosphere-asthenosphere boundaries (LAB)
Highly viscous lithosphere (cold, fluid, melt, and heat-producing element depleted)	Early cratonization and subsequent cooling to increase viscosity	Fast Vs, reflecting cold, dry, refractory composition of mantle lithosphere
High integrated yield strength (or comparatively high relative to surroundings)	Large, equant-shaped cratons surrounded by orogenic belts	Faster seismic velocities of craton relative to those of surrounding mobile belts

The most direct evidence of the time of crust formation comes from U-Pb ages of zircon. These include magmatic zircon that record the crystallization age of the rock, and zircon xenocrysts—either detrital grains or crystals of older rock entrained in younger. Even though the rock in which these zircon grains crystallized may not be preserved, the surviving grains indicate early crust formation. Both igneous and xenocrystic zircons from these and younger Archean rocks also may have strongly negative ε_{Hf} values, another indication of an ancient crustal history (e.g., Griffin et al., 2014; Kemp et al., 2010; Frost et al., 2017). Cratons that have yielded ancient zircons also commonly preserve Pb isotopic evidence of early formation of a craton (Kamber, 2015). Archean rocks exhibit a wide range of $^{207}Pb/^{204}Pb$ ratios at a given $^{206}Pb/^{204}$ ratio. This range is evidence that the rocks were derived from sources that had different U/Pb ratios. Because the decay of ^{235}U to ^{207}Pb is rapid compared to the decay of ^{238}U to ^{206}Pb, crustal and mantle reservoirs had to have formed early in the Hadean or Eoarchean in order to produce the variability in $^{207}Pb/^{204}Pb$ ratio. High $^{207}Pb/^{204}Pb$ initial ratios in Archean rocks reflect derivation from crustal sources with $^{238}U/^{204}Pb$ (μ) that are elevated over coeval mantle values (Kamber, 2015). Sources with these characteristics may be referred to as “high μ” (Oversby, 1975).

The tectonic processes dominating early in Earth history may also favor stability of early-formed cratons. Van Kranendonk et al. (2015) make the case that strong, long-lived cratons formed by vertical tectonics, rather than by accretion through horizontal tectonic processes. They propose that continental blocks formed as thick volcanic plateaus survive because of contemporaneous formation of buoyant mantle roots. Beall et al. (2018) agree that stable cratons may form in a vertical tectonic regime, in which upward transport of melt generates crust with highly depleted lithosphere. However, Beall et al. (2018) point out that this lithosphere would be relatively thin, and that compressive stresses are required to thicken it. The time at which horizontal tectonics began is a matter of debate, but these arguments suggest that Archean cratons formed across this transition, which may have occurred at around 3 Ga (Hawkesworth et al., 2017), may be particularly stable.

A second characteristic that may be associated with craton stability is craton size and shape. A large extent of continental crust and associated mantle lithosphere that is roughly circular will be less susceptible to destruction by processes that work at the edges of continental blocks, such as convective removal or rheological weakening. Although the volume of Archean crust that survives to the present may be less than its original extent, the larger the present-day size of cratons and the more circular rather than elongate their shape, the greater the likelihood that it—or at least its interior—was able to survive tectonic processes that work along cratonic margins to destroy continental lithosphere and recycle it into the mantle.

A third characteristic is the time of cratonization, after which the crust experienced no penetrative deformation, calc-alkalic magmatism, or metamorphism. Most cratons are amalgamations of smaller blocks of crust, sutured along orogens. The time at which this crust ceased to experience penetrative deformation, metamorphism, and calc-alkalic magmatism is defined as their cratonization age. Subsequent cooling will increase the viscosity of the cratonic lithosphere, a characteristic that armors cratons against destruction. Subsequent formation of orogenic belts around the craton may represent weaker zones more likely to take up deformation, further protecting cratons from modification and destruction.

3.2 Geophysical evidence of craton stability

Whereas geologic data for the Archean, although limited, records information about the Earth's ancient past, geophysical techniques can only reveal information about the present-day architecture of cratons. Passive seismic data, recorded during earthquakes, provide some of the greatest insights into the variations within the interior of the earth, including the structure of cratons. Of particular use are seismic tomographic methods, which image of velocity variations that reflect some combination of thermal and/or mineralogical heterogeneities. Resolution can be achieved on a variety of scales from 10s of km, to 1000s of km, depending on frequency of seismic events and spacing of the seismometers. But seismic tomography is an under-determined inverse problem, where various tomographic velocity models can fit the earthquake data equally well. The parameterization and mathematical assumptions vary depending on the tomographer's modeling choices, which results in dozens of models created with different theoretical assumptions and varying resolutions. Variations in earthquake and station density affect coverage of a particular region of the Earth, making it difficult to make direct comparisons of tomographic models from place to place. For this reason, we use both regional models for high-resolution tomography of individual cratons and employ global tomographic models to compare cratons to each other. Primary evidence for stable cratonic lithosphere includes deep lithosphere-asthenosphere boundaries and cratonic lithosphere with fast seismic velocities compared to model upper mantle (Table 1).

4 Geodynamical framework for evaluating craton stability

Not all Archean cratons are underlain by thick lithospheric keels of seismically fast mantle at the present day. Examination of the CAM2016 dVs global tomographic model at 175 km depth suggests that although many cratons retain relatively slow Vs to this depth, others, such as the North China craton and Wyoming craton, have a shallower LAB (Fig. 2). This is a reminder that the properties that control a craton's stability—buoyancy, viscosity, and integrated yield strength—also drive their potential for reworking and/or destruction. Indeed, many studies investigating craton reworking invoke a change to the cratonic lithosphere's composition, rheology, or a combination of the two (e.g., Lee et al., 2011). The premise is that modification is required to change what was once stable to unstable and susceptible to deformation; i.e., the craton experienced change to its material properties post-formation, or a change in its nurturing. There is an alternative premise: perhaps not all cratons were built for longevity. Rather, some cratons could become more susceptible to deformation as the dynamic settings within the mantle changed as the Earth cooled (e.g., Cooper et al., 2006; Beall et al., 2018), i.e., its nature predisposes the craton to modification. Regardless of nature vs nurture, the potential for a craton to be reworked or deformed depends on the interplay between the inherent properties of cratons (composition, rheology, thickness, shape) and the tectonic settings they endure.

4.1 Stability Regime Diagrams

We can explore the relationship between the controls on craton stability and longevity through the use of regime diagrams that map out the conditions for stability versus deformation. For example, the curves in Figures 3 and 4 delineate the parameters that promote lithospheric stability either achieved by enhanced buoyancy or yield stress, respectively. These curves are produced by deriving scaling relationships that describe stability driven by buoyancy (the positive, composition lithospheric buoyancy exceeds the negative thermal buoyancy) or yield stress (the effective yield stress of the lithosphere exceeds convective stresses) (for full details and equations see Cooper et al., 2006). As both thermal buoyancy of downwellings and convective stresses scale with the Rayleigh number, a non-dimensional representation of the strength of convective vigor (Turcotte & Schubert, 2002), it is common to use the Rayleigh number as one of the axes defining the space in regime diagrams. Doing so allows for

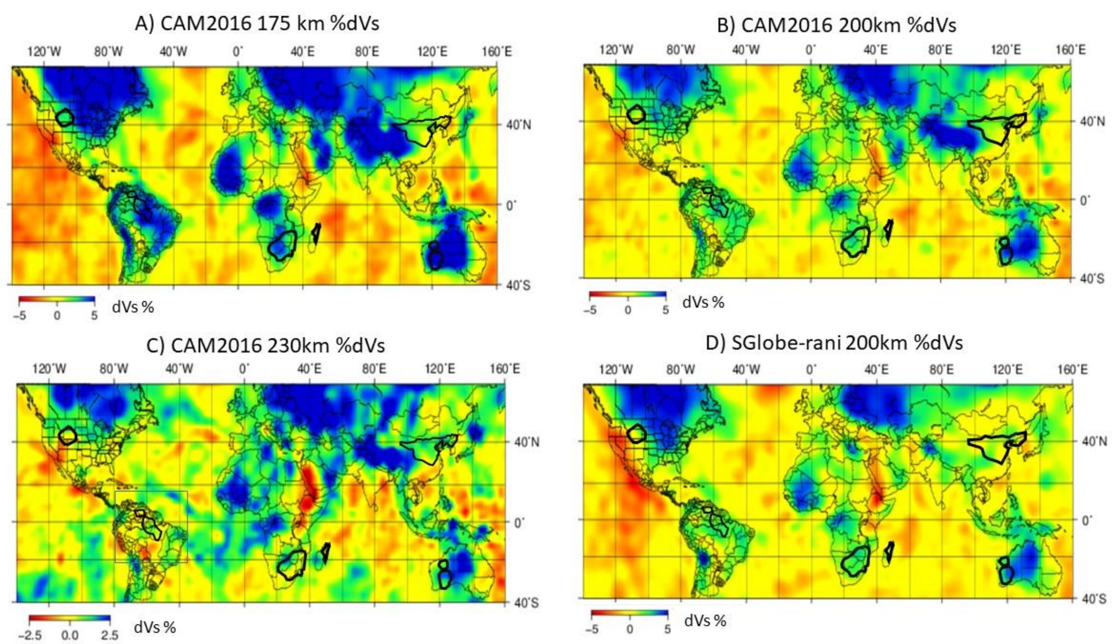

Figure 2. Global tomographic model CAM2016 (Priestley et al., 2019) at (**a**) 175 km, (**b**) 200 km, and (**c**) 230 km depths; and global tomographic model SGlobe_rani (Chang et al., 2015) at (**d**) 200 km depth. Both models display the percentage variation in S-velocity from global averaged 1D velocity model. Archean cratons discussed in the text are outlined in black. Note that although many cratons are underlain by mantle lithosphere with fast seismic velocities at 175 km, some cratons, such as North China Craton and Wyoming, do not show these seismically fast cratonic roots.

comparison across differing dynamic settings as well as providing a proxy for time; the Rayleigh number scales with the internal temperature of the mantle. As the Earth cools from hotter temperatures in the past, the Rayleigh number decreases with time (e.g., Cooper et al., 2006; Sandu et al., 2011). Exploring the connection to the Rayleigh number/time thus introduces the concept of longevity into the stability regimes. The greater the range of Rayleigh numbers over which stability is maintained, the greater the longevity of the craton. We chose lithospheric thickness as the other axis since, again, both scaling relationships depend on it. It also connects back to a primary observable of the cratonic lithosphere that contributes to stability, as well as provides evidence for craton destruction because many proposed mechanisms of craton deformation or destruction are predicated on the removal or of thinning of the lithospheric root.

The regime diagrams in Figures 3 and 4 should be interpreted as follows. Above each curve, the cratonic lithosphere is stable for the combination of parameters within that space. Below each curve, the cratonic lithosphere is unstable, or susceptible to deformation, for the combination of parameters within that space. These scaling relationships were tested against numerical models of lithospheric deformation and matched well the observed transition between deformation and stability within the simulations (Cooper et al., 2006). The parameter space that promotes stability (the area above the curve) changes depending on the material properties of the lithosphere. For example, in Figure 3 increasing values of buoyancy ratios (driven by changes in composition) increases the range of Rayleigh numbers over which the craton will remain stable as well as the range of lithospheric thicknesses that promote stability. This relationship conceptually makes sense. More buoyant lithosphere can more easily compensate or exceed the negative thermal buoyancy of a convective downwelling. Additionally, increasing the thickness of that more buoyant lithosphere adds to the overall buoyancy. This trend follows for variations in yield strength. Figure 4 plots the stability space for variations in the friction coefficient of the lithosphere. Increasing the friction coefficient, which increases the effective yield stress, increases the parameter space over which the lithosphere remains stable. Increasing the lithospheric thickness given the same friction coefficient also increases the effective yield strength, which results in an increase in the range of Rayleigh numbers over which the lithosphere remains stable.

Regime diagrams are powerful because they provide a way to conceptualize the drivers between the transition from stability to deformation as well as a way to quantify the degree of change required to destabilize a once stable region. While viscosity is also a primary control on stability (Lenardic & Moresi, 1999), defining a scaling relationship to explain that behavior is not as straightforward (Cooper et al., 2006). However, we note that enhanced viscosity is built into the assumptions of the yielding scaling relationship in that a minimum viscosity is required for localized failure to occur within the lithosphere (Cooper et al., 2006). In addition, processes that will change the chemical composition (buoyancy) of the lithosphere such as refertilization or

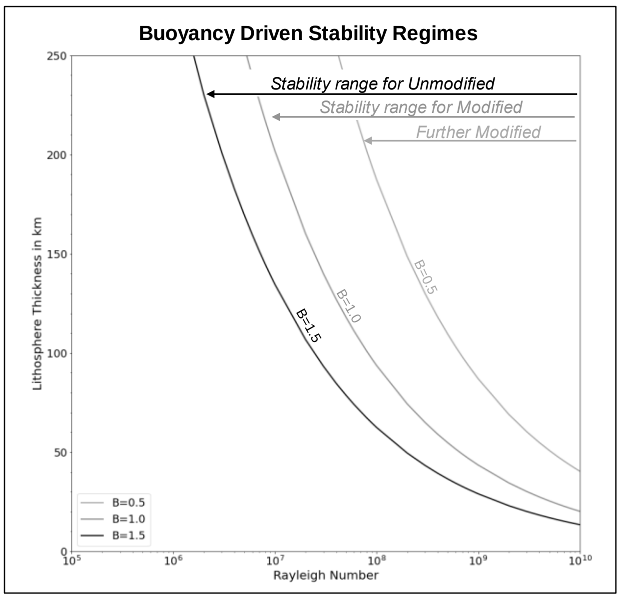

Figure 3. Buoyancy Driven Stability Regime Diagram. Using the scaling relationships derived in Cooper et al. (2006), the curves outline the conditions that promote buoyancy driven stability for cratonic lithosphere for varying Rayleigh number values (non-dimensional number representing convective vigor), continental lithosphere thicknesses, and relative buoyancy ratios of the cratonic lithosphere. Larger values of the buoyancy ratio (B) correspond to an increase in compositional buoyancy of the cratonic lithosphere and smaller values of B indicate less compositionally buoyant lithosphere. Note that B = 0 when cratonic lithosphere has the same compositional density as the convecting mantle. Three scenarios (“Unmodified”, “Modified”, and “Further Modified) on the figure demonstrate the effect that an increase in density driven by modification could have on the range of stability or longevity of the craton.

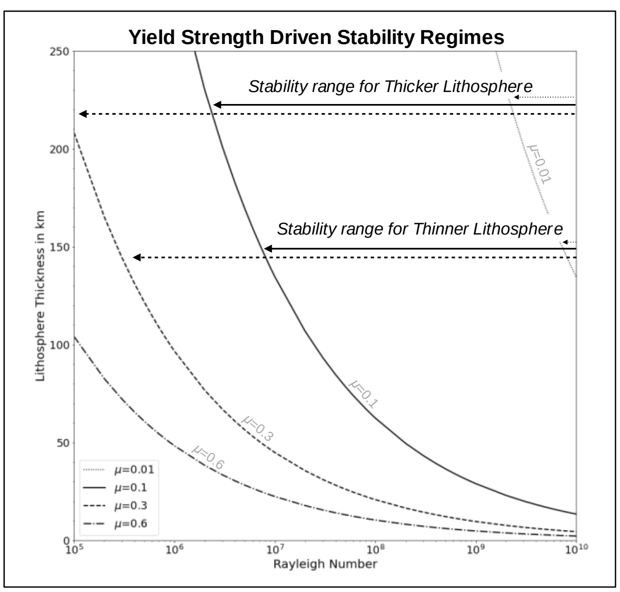

Figure 4. Yield Stress Driven Stability Regime Diagram. As in Fig. 3, scaling relationships derived in Cooper et al., (2006) are used to demarcate the conditions that promote stability driven by the yield stress of the cratonic lithosphere for varying Rayleigh number values, continental lithosphere thicknesses, and friction coefficient values of the cratonic lithosphere. For this stability diagram, the effect of lithospheric thickness in the determination of craton longevity is indicated.

metasomatism will also likely change the viscosity.

Thus, while we cannot use the regime diagrams to provide a framework for variations in viscosity, we can use them to explore how varying buoyancy, yield strength, and lithospheric thickness may lead to deformation. For example, reducing the buoyancy or yield stress of the lithosphere reduces the range of Rayleigh numbers and lithospheric thickness over which the lithosphere is stable. Thus, a cratonic lithosphere of a certain thickness and initial composition which was once stable could experience deformation if its composition (or yield strength) was altered sufficiently enough to place it in a different stability context (i.e., the conditions for stability will be mapped out by a different curve that corresponds to the new composition or yield strength). Similarly, changing the thickness of the cratonic lithosphere in a region moves it into a different location on the stability regime even without changing the buoyancy or yield strength. Increasing the thickness can increase the craton's longevity (the range over Rayleigh numbers over which it will be stable). Decreasing the thickness will either decrease the longevity of the craton, setting the stage for future deformation, or lead to further deformation of the craton.

5 Nature versus Nurture

The regime diagrams suggest that there are two possibilities to explain craton destruction: (1) the craton was not built in a manner that promotes longevity. This circumstance could occur if the craton was not thick, buoyant, or strong enough to be stable over a larger range of dynamic conditions. In other words, destruction was inevitable at some point in Earth's history. (2) The craton was modified such that it no longer maintained either longevity or stability. This scenario proposes that the craton was on the path for longevity, but its material properties (i.e., rheology, composition) were changed by external processes to the degree that made the once stable material now susceptible to deformation. In other words, destruction only became possible after modification to the craton lithosphere. Below we summarize the geologic processes that have been proposed as mechanisms for craton destruction grouped into the categories of nature (inherent) versus nurture (modification).

5.1 Nature

The regime diagrams suggest the theoretical potential that some cratons, but not all, were built in a manner that would promote long term stability or longevity. Stable cratons will have greater lithospheric thickness, greater buoyancy, and higher yield strength, or some combination. Less stable cratons will have thinner lithosphere thickness, reduced buoyancy, lower yield stress, or some combination of the three. These less strong cratons could have been stable post-formation but became subject to deformation as the Earth cooled and the mantle dynamics changed accordingly. Below we discuss proposed hypotheses for craton destruction wherein the inherent, original properties of the craton themselves or rather, the *nature* of the craton, lead to their demise.

5.1.1 Susceptibility to Shearing

Lenardic et al. (2003) argued that the cratonic lithosphere could be destroyed by shearing regardless of enhanced buoyancy and viscosity if the effective yield strength was too low. The shearing in these models occurred along the margins of the cratons where subduction was present. This shearing can progress into the interior destabilizing the craton (Lenardic et al., 2003). In this scenario, the craton's material properties controlling effective yield strength themselves are limiting its stability and do not necessarily require any modifications post-formation. Rather, cratonic lithosphere with too low of values for friction coefficient and cohesion will not possess sufficient yield strength values to overcome stresses driven by subduction along its margins. Unfortunately, lower values of friction coefficient and cohesion are required to create cratons through lithospheric thickening (Cooper et al., 2006), setting up a contradictory premise that the material properties necessary to create cratons may also lead to their destruction. Furthermore, as the effective yield strength is also depth dependent, thinner lithosphere corresponds to weaker lithosphere. Thus, there is also a limiting factor based on thickness: all other properties equal (friction coefficient, cohesion, viscosity and buoyancy), thinner lithosphere is more likely to be destroyed than thicker lithosphere by progressive shearing at its margins.

Shearing could also happen at the base of cratonic lithosphere if the cratonic lithosphere is too thick (Cooper & Conrad, 2009). While it would follow from the regime diagrams that thicker lithosphere always leads to stability and longevity, there could be a limit to craton thickness beyond which it would experience shearing at its base (Cooper & Conrad, 2009). Increasing lithospheric thickness increases the traction stresses at its base (Conrad & Lithgow-Bertelloni, 2006) as well as narrows the convective sublayer, which is the region between the cold rigid craton and the convecting mantle (Cooper et al., 2004). As part of the thermal boundary layer, this region is cooler than the convecting mantle, but not as cold nor chemically depleted as the cratonic lithosphere making it less viscous and more deformable than the craton. As such, the convective sublayer can protect the cratonic lithosphere above by preferentially deforming in response to convective traction stresses. However, if this convective sublayer is too thin, then the increased traction stresses can be transferred into the craton making it more susceptible to deformation. The dual effect of thicker cratonic lithosphere—increased traction stresses and decreased convective sublayer thickness—suggests that there is a maximum craton thickness beyond which the base will be sheared off (Cooper & Conrad, 2009). However, more recent studies suggest that instead of increased potential for deformation, the increase in traction stresses could instead cause cratons to move laterally rather than deform, which then would contribute to increased strain localization in the weaker, surrounding regions (Paul et al., 2019). This transference of strain from cratons to surrounding regions depends on the differential strengths between the cratonic and surrounding lithosphere and it is not clear whether the result would hold if the strength of the cratonic lithosphere within the simulations was reduced.

5.1.2 Proximity to buffer zones

An additional mechanism for craton (in)stability is that the resistance from deformation is not provided by the craton itself, but more its proximity to weaker material (Lenardic et al., 2000). This weaker material, typically younger mobile belts, takes up the deformation during major geologic processes, such as continental collision, much as the crumple zone operates within vehicles. A corollary could be made that cratons that exhibit evidence of deformation were not surrounded by these buffer zones, either originally or the buffer zones had been removed. Without the buffer zones, these cratons were directly exposed to the tectonic events and subject to deformation. Within the buffer zone model, the cratonic lithosphere need not be inherently strong, it just must be stronger than the surrounding buffer zones. Thus, if a weaker craton was once protected by buffer zones that were no longer present, the weaker craton would not necessarily possess the inherent strength necessary for survival. Craton destruction by this proposed mechanism requires either preferential removal of the buffer zones or that the craton was never surrounded by weaker material, but rather directly along a plate boundary. Note, if increased traction stresses due to thick lithosphere does drive strain localization from cratonic lithosphere to weaker surrounding regions (Paul et al., 2019), then this mechanism also acts to buffer the craton from deformation. However, it is not clear how this result would change if the surrounding material was either absent or stronger/weaker or if, as stated above, the cratonic lithosphere was itself weaker.

All of the arguments above demonstrate the potential that not all cratons were built to last and that for some regions destruction was inevitable due to their construction (e.g., lower viscosity, lower buoyancy, weaker yield strength, too thin of lithosphere, too thick of lithosphere, lack of armoring by surrounding buffering material).

Now, we turn our attention to the scenarios in which cratons originated with the potential for long-lived survival but encountered tectonic settings which changed their original nature in a manner making deformation and destruction possible.

5.2 Nurture

The characteristics that make cratonic lithosphere strong also suggest the processes that may weaken it and lead to modification and destruction of cratons. For example, if cratonic lithosphere gains its strength in part due to a temperature-dependent rheology and cooler thermal structure, then it may be weakened by heating, for example by the arrival of a deep mantle plume or other anomalous thermal upwellings (e.g., Davies, 1994). Or, if cratonic lithosphere is chemically buoyant due to melt depletion during its formation (e.g., Lee et al., 2005), its density structure may be altered by infiltration of partial melts or metasomatism. Furthermore, if the cratonic lithosphere is also compositionally rheologically strong due to dehydration (e.g., Lee et al., 2005), rehydration via metasomatism could reduce its viscosity and weaken the material. Perturbing those properties that promote stability (rheology and composition) provides the means for destabilization. Thus, *nurture* mechanisms call upon events within a cratonic region's geologic history that introduce conditions that will modify the material properties that once promoted stability. Below we outline several proposed mechanisms that could alter the lithospheric material properties and lead to craton modification and destruction.

5.2.1 Subduction

A commonly proposed mechanism of craton destruction is interaction with subduction zones. Subduction zones are invoked in these hypotheses not necessarily to induce shearing along the margins as in Lenardic et al. (2003), but as means of delivering hydrating fluids to the craton lithosphere, either on their own (e.g., Humphreys, 1995) or by inducing flow patterns (e.g., Kusky et al., 2014). These fluids then rehydrate the cratonic lithosphere reducing its viscosity and buoyancy resulting in greater potential for deformation (e.g., Lee et al., 2011). The release of hydrating fluids from a subducting slab has been used as an explanation for weakening the overriding plate, inducing delamination of the lithosphere as well as widespread melting (Humphreys, 1995). This mechanism requires flat slab subduction, which extends the impact of the dehydration reactions occurring within the slab laterally further into the interior of the overriding plate (Humphreys, 1995). As the flat slab founders, the newly hydrated lithosphere is then subjected to hotter upwelling mantle flowing in and around the slab (Humphreys, 1995). This heat pulse then induces magmatism in the region (Humphreys, 1995). An alternative model suggests that subduction zones stall out along the top of the transition zone hydrating the mantle above it (Kusky et al., 2014). As the slab rolls back, suction forces drive mantle flow upward and toward the craton lithosphere inducing melting of the hydrated mantle (Kusky et al., 2014). These partial melts metasomatize and thermochemically erode the cratonic root (Kusky et al., 2014). This process replaces the lost cratonic material with more fertile mantle compositions (Kusky et al., 2014).

Both models rely on subduction zones as transporters of hydrous fluids and significant drivers of mantle flow. They also both provide specific predictions of expected observations - evidence of rehydration of the lithosphere followed by anomalous heating. Although it may be unclear how to delineate between the two proposed mechanisms, this sequence in the rock record could indicate interaction with a subduction zone that drove craton destruction.

5.2.2 Metasomatism associated with MLDs

One interpretation of mid-lithospheric discontinuities is that they represent accumulations of seismically slow minerals such as phlogopite, amphibole, pyroxene, and carbonates in veins and layers marking the extent of metasomatism within continental lithosphere (Selway et al., 2015; Aulbach et al., 2017). Liu et al. (2018) suggest that mid-lithospheric discontinuities

(MLDs) are a possible locus for delamination of cratonic lithosphere. If the seismically visible discontinuities represent regions of preferential accumulation of metasomatic minerals or water-enriched peridotite, then these layers would be relatively weaker than surrounding regions and could be the layer along which delamination could occur. Their simulations suggest that if the MLD edge does not abut strong and cold lithosphere, then edge failure can induce rapid keel delamination along an MLD layer. While an intriguing proposal, this mechanism does not adequately explain both the ubiquity of MLDs within cratonic lithosphere and the continued persistence of the associated thick lithosphere (e.g., Cooper et al., 2017), so the global significance of this mechanism is unknown.

5.2.3 Plumes

Interaction with mantle plumes could also provide the means to modify the thermal structure and material properties of cratonic lithosphere leading to craton destruction (e.g., Lee et al., 2011). In this proposed mechanism, thermochemical plumes heat the cool, cratonic lithosphere affecting its temperature-dependent rheology and causing a reduction in viscosity (e.g., Wu et al., 2019). The plumes can also provide magma and metasomatizing fluids that could rehydrate and refertilize the composition of the cratonic lithosphere, changing the rheology and buoyancy and making it more susceptible to dripping and/or delamination (e.g., Liao et al., 2017). Finally, the thermochemical plumes could also introduce pathways for melt migration that would also reduce the overall strength of the cratonic lithosphere making it more susceptible to future deformation (Foley, 2008). These plume-driven processes could also eventually replace the once-depleted cratonic lithosphere with more fertile compositions (Hu et al., 2018), changing the overall buoyancy of the region.

However, melting driven by plumes requires that the mantle solidus is crossed during decompression. Thick cratonic lithosphere may limit this requirement by impeding the upward trajectory of plume material (Lee et al., 2011). Melting could more easily occur in regions with thinner lithosphere that allow for more head room for the plume to ascend (Lee et al., 2011). If, however, the plume and thick cratonic regions were locked relative to each other, the thicker cratonic lithosphere could be locally heated by the plume, which would reduce the degree of decompression needed for melting to occur (Lee et al., 2011). Yet, the dependence of plume-driven melting on lithospheric thickness could perpetuate initial thickness variations with regions within the craton with thinner lithosphere more susceptible to modification and deformation and further thinning, while thicker cratonic roots maintain their thickness.

5.2.4 Rifting

Another path to craton destruction could be provided by lithospheric thinning during rifting episodes (i.e., Griffin et al., 2003). Over their long geologic history, cratons likely experienced rifting, particularly associated with the breakup of supercontinents (e.g., Merdith et al., 2019). Rifting could lead to thinning of the cratonic lithosphere, which in turn would increase the likelihood of further deformation. Whether it is the cratonic lithosphere itself that thins during rifting rather than surrounding lithosphere depends on rheology contrasts between the two materials (Wenker & Beaumont, 2018b). Geodynamic simulations demonstrate that unless the cratonic lithosphere has been sufficiently weakened by metasomatism, then rifting remains focused and isolated in the surrounding lithosphere (Wenker & Beaumont, 2018a). This result suggests that rifting alone is not sufficient to explain cratonic destruction, but may exacerbate deformation if the cratonic lithosphere had been previously modified and weakened.

5.2.5 Progressive refertilization

Finally, the last mode of modifying the material properties of cratonic lithosphere takes advantage of its extended geologic history. The long-lived nature of cratons suggests then that they have a longer period over which to accumulate repeated episodes of metasomatism or progressive refertilization (Griffin & O'Reilly, 2007) that drives gradual increases in the density of the cratonic root (Lee et al., 2011). The increase in density can then drive subsidence of the craton as well as potentially set the stage for future delamination driven by gravitational instabilities (Liu et al., 2019).

All of the above modification processes may occur alone or in combination. Indeed, some studies have shown that such combinations are required to destabilize cratonic lithosphere and to explain the geologic observations in the region (e.g., Wang et al., 2016). Distinguishing between the proposed nurture and nature mechanisms requires an in-depth analysis and comparison of modified versus undeformed cratons to look for commonalities in their geologic histories as well as summarizing the expected evidence for craton modification and destruction.

6 Evidence for Modification

6.1 Geologic evidence of craton modification

The processes described above that may destabilize and destroy cratonic lithosphere may be recorded in the geologic record, as described below and summarized in Table 2. Recent lithospheric processes are more likely to have preserved geologic evidence that can be accessed on the surface than are processes that took place in the more distant past.

Table 2
Summary of processes that modify cratons and evidence for destruction

Process	**Geodynamical Effect**	**Geological evidence**	**Geophysical evidence**
Subduction and slab rollback	Heat and hydrating fluids reduce viscosity and buoyancy	Migrating calc-alkalic convergent margin magmatism and sedimentation	Slow S-velocity
Metasomatism	Introduces fluid and melt to lithosphere, weakening it. Can be cumulate, as in “progressive refertilization”	Evidence from xenoliths, alkalic magmatism, and possibly subsidence and basin formation	Some MLD may form by this process
Plumes	Heat and mantle-derived magma reduce viscosity and buoyancy	Large igneous provinces	Slow S-velocity
Rifting	Thins lithosphere, provides pathway for heat and fluids	Extension, volcanism, syn-rift sedimentation	Shallower LAB

- ***Subduction zones*** typically are associated with calc-alkalic, relatively oxidized arc magmas that form arc batholiths and volcanoes dominated by granodiorite and basaltic andesite and andesite respectively (Frost & Frost, 2019). The geologic record may also preserve belts of high pressure-low temperature metamorphic rocks along the subducting plate that result from the subduction of cool oceanic crust to mantle depths (Oxburgh & Turcotte, 1971).
- ***Flat-slab subduction*** may be recorded by a geographic sweep of magmatism and sedimentation accompanying slab retreat and steepening (rollback) (Best & Christiansen, 1991; Cassel et al., 2018). Flat slab subduction also may release fluids that hydrate and metasomatize the mantle peridotite above the slab. Subsequent rollback or foundering

and an influx of hot asthenosphere causes this metasomatized mantle to partially melt, forming potassic, alkaline magmas (Feeley, 2003). It is important to emphasize that the metasomatism must precede the generation of the alkaline melts, in some cases millions of years before, such that connecting the alkaline rocks to the subduction-related metasomatism can be difficult.

- ***Metasomatism and refertilization*** of sub-cratonic mantle can be inferred from the composition of magmas formed by partial melting of that mantle lithosphere, as described above. More direct evidence is provided by mantle xenoliths. In addition to recording the temperature and pressure at which the minerals in the xenolith equilibrated, the major and trace element compositions can be used to identify processes such as Si-enrichment by silicic melts or metasomatizing fluids (Lee et al., 2011). Isotopic systematics can indicate the timing of metasomatism (Carlson et al., 2004). Liu et al. (2019) suggest another possible geologic signal of refertilization: they propose that subsidence and basin formation may result from metasomatism of subcratonic mantle lithosphere and subsequent cooling and gradual increase in density.
- The presence of ***mantle plumes*** also may be recognized by the magmas that form. A linear, time-progressive track of tholeiitic and alkali basalt characterizes plume magmatism impinging beneath oceanic plates, and bimodal ferrroan, alkali-calcic magmatism results from the passage of a continental plate across a plume (i.e., McCurry et al., 2008). Where erosion has removed plume-related volcanic rocks, the plume track may be identified by time-progressive bimodal intrusive suites (i.e., McHone, 1996).
- ***Rifting***, which by thinning the lithosphere, can provide a pathway for heat and fluids, also may be recognized in the geologic record by magmatism and by syn-rift sedimentation, commonly interbedded with volcanic rocks (e.g., Chapin & Cather, 1994). Rift-related volcanism may be associated with broad areas of extension, such as in the Basin and Range in southwestern United States, or in narrower rifts. Igneous rocks range from tholeiitic to alkaline and from basalt to rhyolite, depending on the rate of extension, the degree of partial melting of the mantle source, and variations in the composition of the mantle source (Frost & Frost, 2019).

6.2 Geophysical evidence of craton modification

This study evaluates evidence from both global and regional tomographic models. Global models are used to compare the velocity structures of the different cratons to each other. From the many global models that are available, we selected two, SGlobe_rani (Chang et al., 2015) and CAM2016 (Priestly & Ho, 2016), as having the best uniform coverage of the cratons of interest, and the resolution and parameterization that allow tectonic insights at the cratonic scale. These two models are compared on Figure 2, which show global S-velocities at a given depth as deviations from an average model. The results for SGlobe_rani and CAM2016 at 200 km (Fig. 2bd) give similar results. The Australian Archean cratons, Pilbara and Yilgarn, show faster velocities than the southern Africa Archean cratons and Amazonia and all have positive dVs% compared to the global average. Other cratons, such as Wyoming and North China, display minimally faster dVs than the average model, as indicated by yellow and yellow-green colors. Examination of %dVs at varying depths helps to constrain the depth of the LAB, by revealing the depth to which fast seismic velocities characteristic of cratonic lithosphere persist beneath cratons. For example, of the cratons outlined on Figure 2, Pilbara and Yilgarn retain the fastest S-velocities at a depth of 230 km, indicating their cratonic roots extend at least to this depth (Fig. 2c). Global LAB maps (e.g., Cooper et al., 2017) align well with global tomography models, and confirm that there is considerable variation in the thickness of Archean cratonic keels at the present day.

Regional tomographic models provide more details into velocity variations on a smaller (~100 km) scale. For example, Figure 5 compares the dVs global tomographic model, SGlobe_rani with regional model WUS, showing depth slices at 100, 150, 200, and 250 km within the region of the Wyoming craton. Note that the global model does not resolve well established features that are clearly imaged by the regional model, such as the Yellowstone hotspot and eastern margin of the Basin and Range. This comparison illustrates the value of regional models in investigating individual cratons, although they cannot be compared to other regional models to global models due to the variation in theoretical, data, and parameterization choices and effects of local geologic variations.

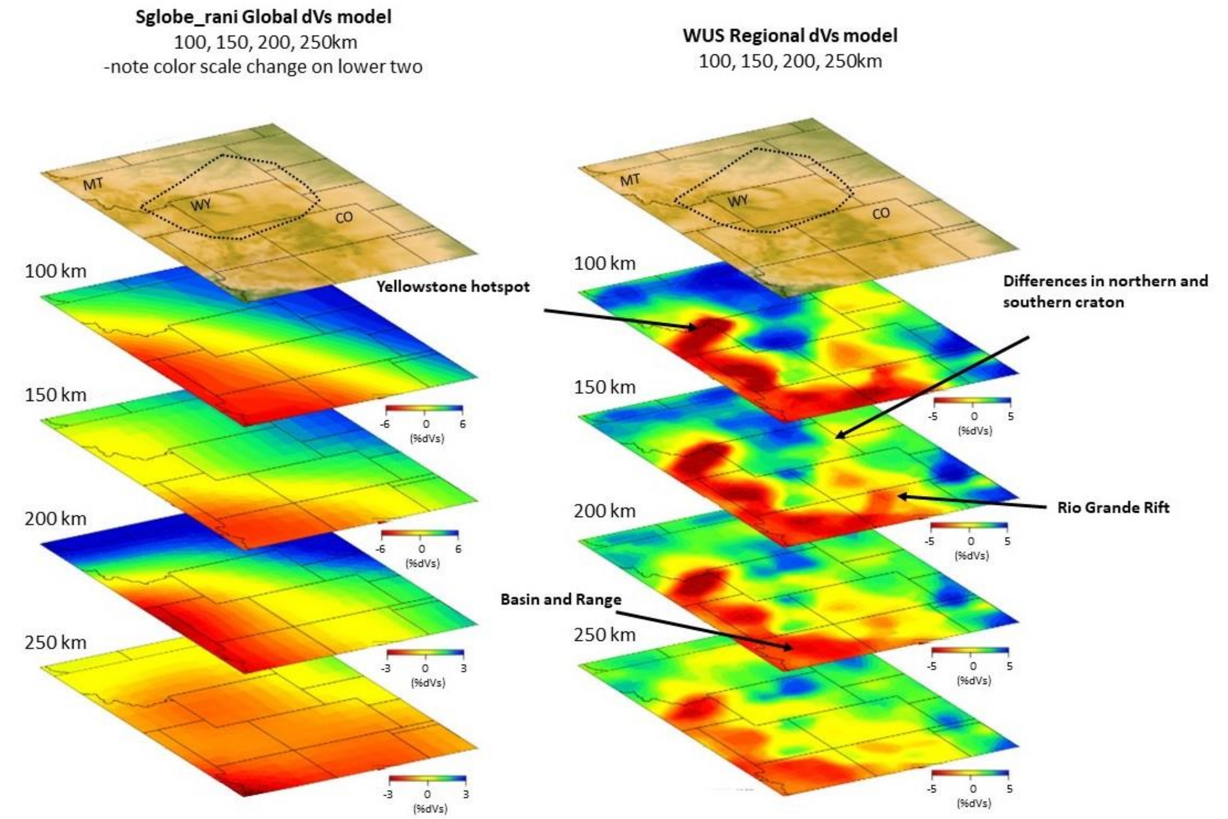

Figure 5. Comparison of global model, Sglobe_rani (Chang et al., 2015), and regional model WUS (Schmandt and Humphreys, 2010). Both models show %dVs with depth slices of 100, 150, 200, and 250 km. The Wyoming craton is outlined, and regional features are highlighted.

1D tomographic models of the velocity structure beneath cratons can be constructed from regional or global models. To interpret these, it is helpful to compare a typical cratonic profile to an average Earth profile (Fig. 6cd). Model mantle lithosphere to a depth of 200 km has a S-velocity of 4.5 km/s, then it gradually increases as the mantle becomes warmer with depth (Fig. 6d). By contrast, stable cratonic roots have faster Vs, as illustrated by profiles constructed beneath the Pilbara and Yilgarn cratons (Fig. 6c). These profiles have a characteristic inflection at the base of the cratonic mantle lithosphere, at around 200 km. Although the differences in the profiles may seem small, it is important to remember that a relatively small velocity increase of 1% can be attributed to significant differences in composition (5% increase in molar Mg/(Mg + Fe^{2+}) x 100, or Mg#), or temperature (220°C decrease) (Lee, 2003).

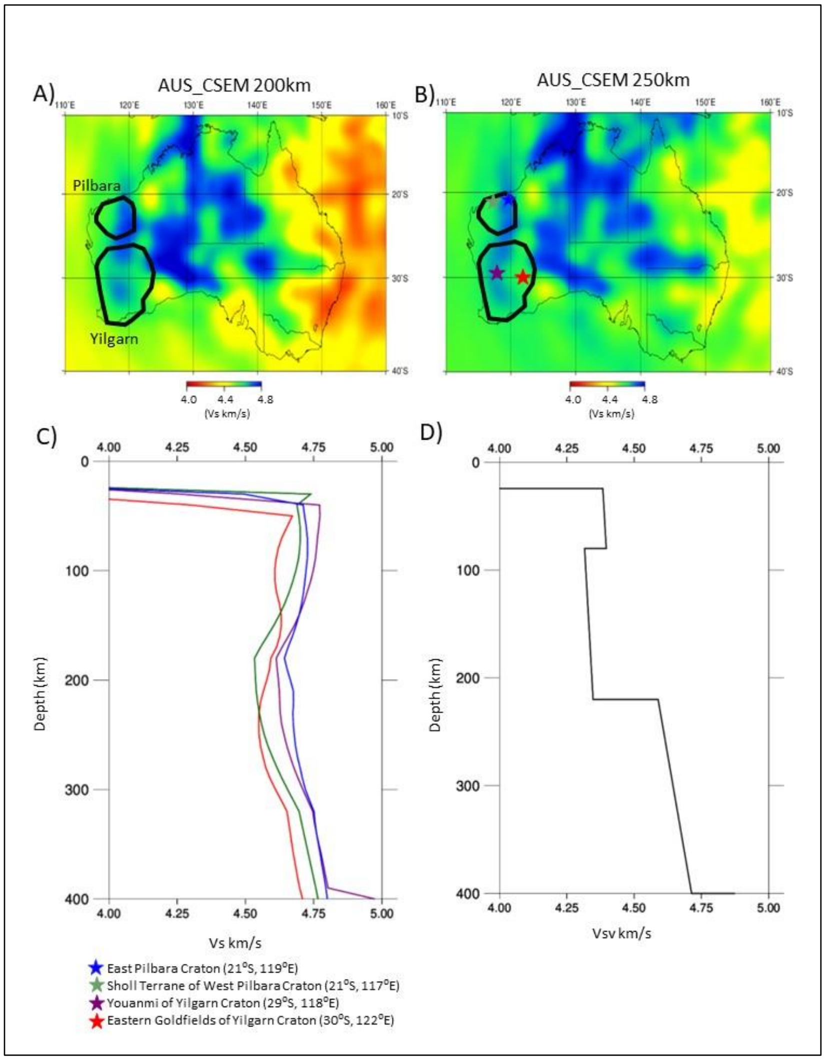

Figure 6. Depth slices and 1D models through the Australian CSEM model (Fichtner et al., 2018) highlighting variations in the Pilbara and Yilgarn Archean cratons. (**a**) S-velocity depth slice at 200 km; (**b**) S-velocity depth slice at 250 km, with location markers for 1D models; (**c**) 1D S-velocity model to 400 km depth taken at four locations in the stable Archean cratons; (**d**) PREM background velocity model for Sv-velocities (Dziewonski and Anderson, 1981).

7 Case Studies

If the main controls on the stability and longevity of a craton relate to its formation—for example, the composition of its crust and mantle lithosphere and the tectonomagmatic processes that formed them—then these controls may emerge from a comparison of stable and modified cratons. On the other hand, if the alteration of the Archean cratons is a result of the processes to which it has been subject--how it has been nurtured--then the tectonic events surrounding that craton must also be identified and understood. We have chosen cratons to represent each type that are well-described geologically and geophysically. We compare and contrast the geological and geophysical properties of these cratons to better understand the relative importance of nature vs. nurture. The stable Archean cratons discussed below are the Pilbara and Yilgarn cratons in western Australia, and the Zimbabwe and Kaapvaal cratons in Africa. The Wyoming and North

China Craton are well-documented modified Archean-age cratons, and we include a brief discussion of the Amazonian and Madagascar cratons, which have been suggested to be modified but are not as well understood.

7.1 Stable cratons

7.1.1. Pilbara and Yilgarn cratons

The geologic histories of these cratons suggest that they are favored for long-term stability. The Yilgarn craton of western Australia is composed of an old continental nucleus, the 3.0-3.2 Ga Youanmi Terrane, which occupies the western half of the craton (Fig. 7a). The Narryer Terrane to the north is in fault-contact with the Youanmi Terrane and includes the Jack Hills metasedimentary belt, which was deposited between 3.05 Ga and 2.65 Ga (Rasmussen et al., 2010). Some 7% of the more than 100,000 detrital zircon grains dated from this quartzite are between 3.8 and 4.4 Ga (Nebel et al., 2014). The Eastern Goldfields Superterrane to the east is also in fault contact with the Youanmi Terrane. It is younger than the other subprovinces, and is composed of 2720-2660 Ma greenstones and voluminous 2720-2620 Ma granitic rocks. Magmatism and deformation in the Eastern Goldfields Superterrane ceased in the Neoarchean, at

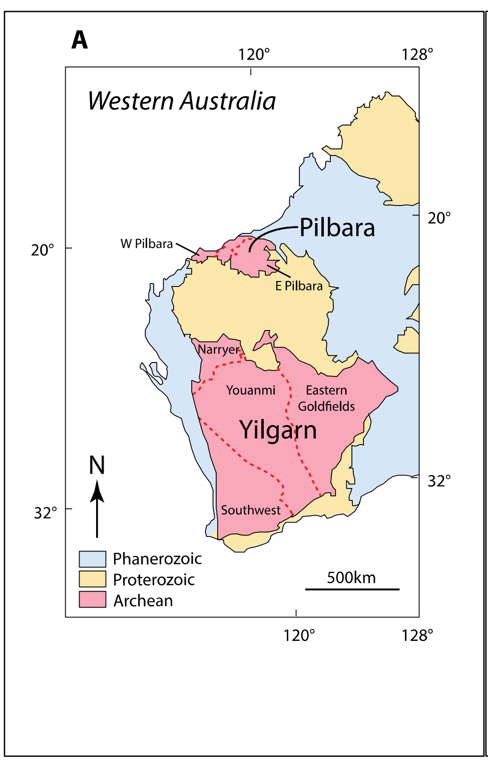

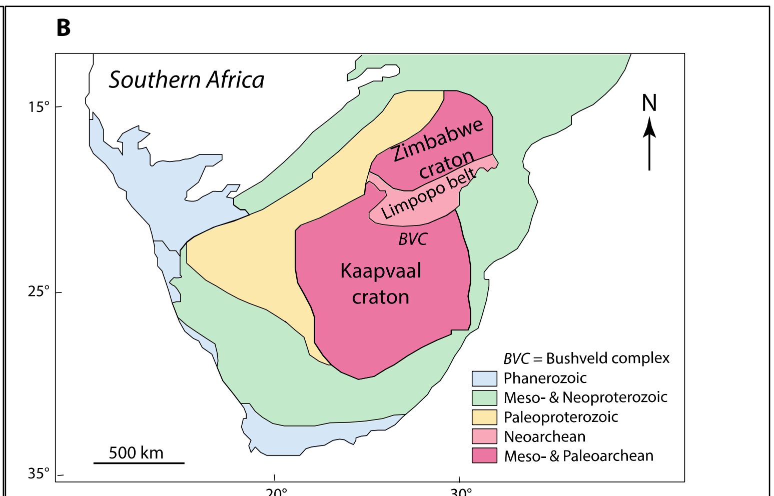

Figure 7. Geologic sketch maps of some stable cratons. Pilbara and Yilgarn cratons in Australia and Zimbabwe and Kaapvaal cratons in southern Africa are examples of Archean cratons that preserve thick cratonic mantle lithosphere. Dashed red lines indicate limits of Archean terranes within each craton. Craton boundaries from Cawood and Korsch (2008) and Jacobs et al. (2008).

2.63 Ga (Van Kranendonk et al., 2013).

The Pilbara craton of western Australia is better exposed than the Yilgarn craton and preserves an extensive Paleoarchean history. Evidence of even older crust is restricted to 3.73-3.70 Ga inherited zircon in a single eruptive unit (Petersson et al., 2019). The Eastern Pilbara Terrane (Fig. 7a) is composed of rocks 3.53 to 3.17 Ga in age and exhibits domal granite-greenstone structures interpreted to have formed during multiple partial convective overturn events (Van Kranendonk et al., 2019). The Western Pilbara Superterrane is composed of three terranes: the 3.20 Ga Regal terrane dominated by MORB-type basalts, the 3.27 Ga Karratha Terrane, which may represent a fragment of the East Pilbara Terrane, and the 3.13 Ga Sholl Terrane, composed mainly of juvenile arc-type volcanic rocks. The west Pilbara Superterrane and East Pilbara Terrane may have been amalgamated during the ca. 3070 Ma Prinsep orogeny, and certainly prior to the deposition of the Cleaverville Formation, which is correlated across the craton, at ca. 3020-3015 Ma (Sheppard et al., 2017).

The PIlbara and Yilgarn cratons came together at 2.0 Ga along the Capricorn orogen to form the core of an amalgamated West Australian craton that was part of Supercontinent Nuna (Cawood & Korsch, 2008). The West Australian craton was joined with the Northern Australian continent along the Paterson orogen at ~1.8 Ga, then following further amalgamation, a more extensive Australian continent was sutured to the Mawson craton of Antarctica by 1.2 Ga to form part of Rodinia (Cawood & Korsch, 2008). The Western Australian craton continued to occupy a position in plate interiors during the breakup of Rodinia and formation and dispersal of Pangea (Scotese & Elling, 2017). Thus the Yilgarn and Pilbara cratons have not been near a convergent plate margin since the Paleoproterozoic, and their position in plate interiors may have protected these cratons and their mantle roots from deformation or destruction associated with subduction.

Global summaries of lithospheric thickness suggest that the LAB lies more than 200 km beneath Pilbara and Yilgarn (Cooper et al., 2017). In a regional model, Fishwick et al. (2005) employed surface wave tomography methods to the Australian continent to model the lithospheric variations. In this model, fast S-wave velocities are imaged to depths greater than 150 km beneath the Yilgarn and Pilbara cratons. These faster S-wave velocities are expected in an Archean craton that has been stable through time and corroborate global models that identify a cool and chemical buoyant root beneath western Australia. A more focused study of the Yilgarn craton combining 2D seismic profiles, 1D receiver functions, and 3D seismic tomography, revealed lithosphere existing beneath the craton to approximately 220 km depth (Goleby et al., 2006). Another regional study of the Australian lithosphere resulted in the AuSREM mantle model (Kennett & Salmon, 2012), which also revealed thicker lithospheric keels beneath the Archean cratons, to depths exceeding 150 km. The CSEM-Australasia tomographic model is one of the latest models published in the Australian region (Saygin et al., 2019). This model is part of the Collaborative Seismic Earth Model (CSEM) project by Fichtner et al. (2018) and was created by using both spectral-element and full waveform inversion and modelling methods, first used by Fichtner et al. (2006, 2009). The CSEM-Australasia model outputs for two S_v depth slices at 200 km and 250 km are displayed in Figure 6ab, as well as a depth profile of the velocities through four regions of the Pilbara and Yilgarn cratons. Both depth slices (Fig. 6ab) show that most of western Australia displays relatively faster velocities typical of cratons and that both Pilbara and Yilgarn maintain their faster velocities to below 200 km. The interior of Australia east of the Pilbara and Yilgarn craton also displays a faster velocities. Within the Archean cratons, finer detail of the specific regions can be observed in Figure 6c, where continuous depth profiles of the velocities are shown for four regions of the Archean cratons: 1) the Eastern Pilbara Craton; 2) the Sholl Terrane of the western Pilbara Craton; 3) the Youanmi Province of the Yilgarn Craton; and 4) the Eastern Goldfields of the Yilgarn craton. The East Pilbara, Sholl Terrane and Youanmi Province reveal typical cratonic profiles, with a convex shape to the upper ~200 km. The Eastern Goldfields region shows a slightly different, more concave profile in the upper 150 km with lower seismic velocities than would typically be expected in a stable cratonic region. This may relate to the fact that the Eastern Goldfields Superterrane is the youngest part of the Yilgarn craton and is proposed to have formed after thick lithosphere was already present beneath the rest of the craton. Abundant Neoarchean komatiites have been interpreted as forming from a mantle plume that ascended to shallower levels along the margin of the older Youanmi terrane (Mole, 2014).

7.1.2. Zimbabwe and Kaapvaal cratons

The Zimbabwe and Kaapvaal Archean cratons (Fig. 7b) are part of a larger Precambrian land mass composed of Archean and Proterozoic crustal blocks assembled over a prolonged period. Three Archean cratons compose its core: the Zimbabwe and Kaapvaal cratons in southern Africa, and the Grunehogna craton in east Antarctica. Of these, only the Zimbabwe craton retains

Pb isotopic evidence of forming from sources extracted early from the mantle (Taylor et al., 1991; Berger & Rollinson, 1997) but both Zimbabwe and Kaapvaal have ancient histories. The Kaapvaal craton formed by amalgamation of the ~3.7 Ga Witwatersrand and 3.2 Ga Kimberley blocks at around 2.9 Ga (Schmitz et al., 2004). The Zimbabwe and Kaapvaal cratons were assembled along the Limpopo belt at 2.7-2.65 Ga (Zeh et al., 2009). The Zimbabwe and Kaapvaal cratons were joined to the Grunehogna craton by 1750 Ma to form a proto-Kalahari craton (Jacobs et al., 2008). Subsequent accretion of continental arcs along the northwest margin took place between 1.4 and 1.2 Ga, followed by arc accretion and continental collision between 1.10 and 1.05 Ga on the south and east. These Proterozoic crustal additions doubled the craton in size, forming the Kalahari craton.

Xenolith evidence suggests that the Kaapvaal mantle lithosphere was metasomatized several times during its history. Based on Re-Os ages, the first event took place at around 2.9 Ga and resulted in variable silica enrichment (Carlson et al., 1999). This metasomatism corresponds to the time western and eastern Kaapvaal blocks were accreted, leading Simon et al. (2007) to suggest that Si-rich fluids may have been released from a subducting slab. A second event that may have affected the composition of the subcratonic mantle is the intrusion of the world's largest layered mafic intrusion, the Bushveld intrusion, at 2.06 Ga (Rajesh et al., 2013). Mantle xenoliths and inclusions in diamonds suggest that the mantle lithosphere beneath the Bushveld intrusion was metasomatized by basaltic melt at this time (Richardson and Shirey, 2008; Carlson et al., 2005; Shirey et al., 2003). Emplacement of dikes related to the ~180 Ma Karoo plume (Youssof et al., 2015) may have affected the southern Kaapvaal craton (Celli et al., 2020a). Xenolith data also document local metasomatism associated with kimberlite magmatism between 120-90 Ma (Simon et al., 2007).

Despite a number of events that modified or had the potential to modify the Zimbabwe and Kaapvaal cratons since their formation, they exhibit geophysical characteristics typical of stability on regional tomographic models. The depth of the lithosphere beneath the Kaapvaal craton has been seismically imaged to depths of 300-350 km (Youssof et al., 2015). The recent regional tomographic velocity model Africa.ENT (Emry et al., 2018) displays a fast S-velocities of up to 4.8 km/s in the upper 300 km of the mantle beneath the Kaapvaal craton. These faster, cratonic velocities can be observed in both the depth slices at 210 km, 260 km, and in the 1D Vs profiles of Figure 8. This regional model does not resolve lithospheric features associated with the Bushveld intrusion, but the LImpopo Belt, along which Kaapvaal and Zimbabwe were joined

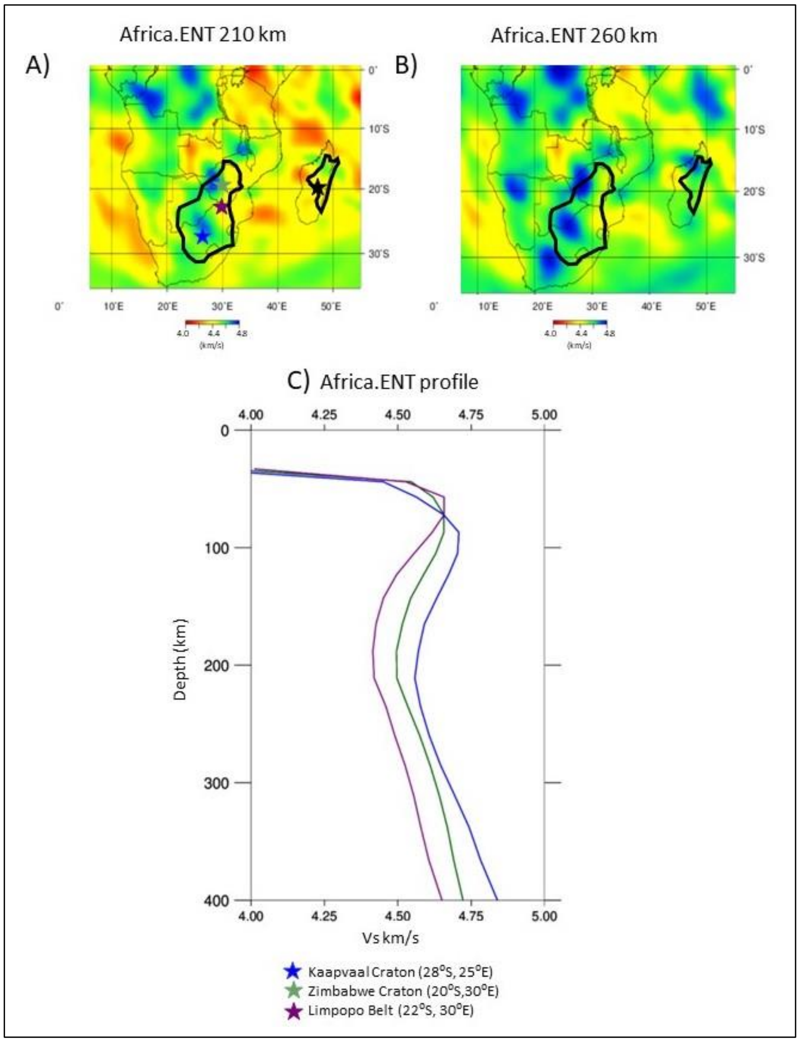

Figure 8. Depth slices and 1D S-velocity models through the African ENT tomographic model (Emry et al., 2018) highlighting variations in the Archean cratons. (**a**) depth slice at 210 km; (**b**) depth slice at 260 km, with location markers for 1D models; (**c**) 1D S-velocity model to 400 km depth from locations within the Kalahari craton.

in the Neoarchean, appears to have slightly thinner cratonic lithosphere than either Zimbabwe or Kaapvaal cratons.

7.2. Modified cratons

7.2.1. North China craton

Although Archean exposures are limited in the North China craton (NCC), Eoarchean or Hadean zircons have been documented from eastern, southern, and central areas (Wan et al., 2019). A high μ Pb isotopic signature has been documented for Paleoarchean rocks in the eastern NCC, consistent with early crust formation (Wan et al., 1997; Kamber, 2015). The NCC is composed of eastern and western blocks (Fig. 9a). The western block is composed of two

Archean areas joined along the Paleoproterozoic khondalite belt, which is interpreted as a 2.0-1.9 Ga collisional orogen that joined northern and southern areas to form the western block. The eastern block of the NCC also consists of two Archean terranes joined along the Paleoproterozoic Jiao-Liao-Ji belt (Zhao et al., 2005). Metamorphism of this belt occurred at ~1.9 Ga. It has been interpreted as a collisional belt or alternatively as formed by opening and closing of an intracontinental rift (Zhao et al., 2005). The eastern and western blocks of the NCC evolved separately during the Archean and were amalgamated at ~1.85 Ga along the Trans-North China Orogen, a belt composed of oceanic arcs, subduction accretion complexes, back-arcs and foreland basins (Polat et al. 2006; Xu et al., 2018). The NCC is surrounded by younger orogenic belts: the Central Asian orogenic belt to the north, Qilianshan-Qinling-Dabie and Central China orogens to the southwest, and the Sulu belt/Imjingang orogen to the southeast (Zhao et al., 2005).

The NCC was part of the Nuna supercontinent until it broke apart in the Mesoproterozoic (Zhang et al., 2012).

The North China craton was one of the first cratons recognized to have undergone destruction of its cratonic root (Menzies et al, 1993). Evidence from peridotite xenoliths brought up in diamondiferous kimberlite in the eastern NCC suggests that a thick, refractory subcratonic mantle lithosphere was established in the Archean (Gao et al. 2002; Chu et al., 2009) and persisted through the Ordovician under at least some parts of the NCC (Zheng et al., 2005). Extensive Early Cretaceous magmatism is associated with flat-slab subduction of the Paleo-Pacific plate along the eastern margin of the craton (Kusky et al 2014; Wang et al., 2019). Evidence from mantle xenoliths in Cenozoic basalts suggests that the lithosphere beneath the eastern NCC was thinned by this time (Zheng et al., 2005; Chu et al., 2009).

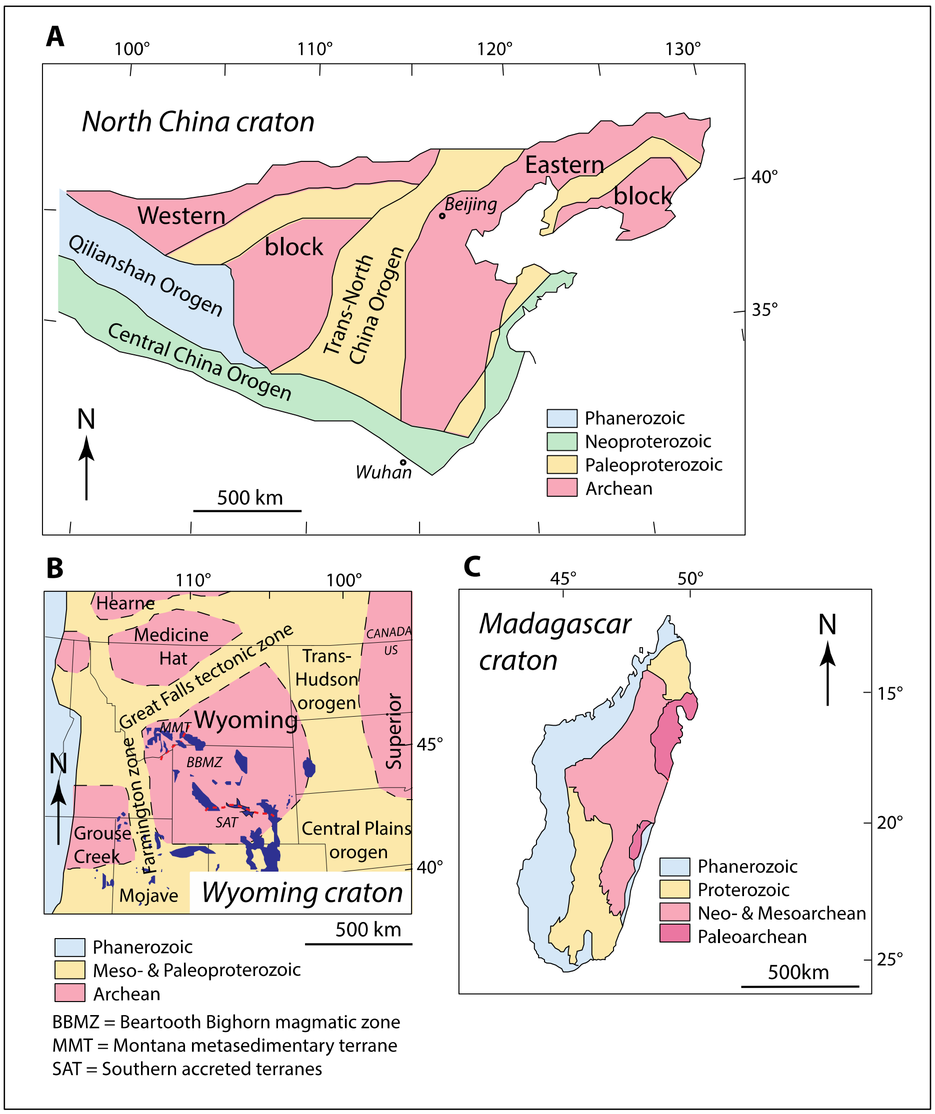

Figure 9. Geologic sketch maps of cratons that may have been modified. (**a**) The North China craton, (**b**) Wyoming craton, and (**c**) Madagascar craton are examples of cratons that today exhibit geophysical characteristics that have been interpreted to suggest that they may have lost all or part of their original subcratonic mantle lithosphere. Wyoming craton sub-provinces are delineated with dashed red lines. Craton boundaries from Xu et al. (2018), Foster et al. (2006), and Tucker (2014).

Global tomographic model CAM2016 reveals the lack of a cratonic root beneath the NCC at 175 km (Fig. 2). Finer tomographic detail is imaged by a well-resolved regional model, FWEA18 (Tao et al., 2018), as displayed in Figure 10. The FWEA18 model jointly inverts for Vpv, Vph, Vsv, Vsh, and density in the mantle beneath the NCC (Tao et al., 2018). Both the Vp and Vs models (Fig. 10ab) reveal that the eastern NCC is dramatically slower than the western NCC. This variation between the western and eastern portions of the craton extends from the uppermost mantle down to depths of 250-300 km, coinciding with expected cratonic thicknesses of Archean cratons. 1D S-velocity profiles through the Ordos basin in the southern part of the western NCC and Archean age rocks near Qinhuangdao in the eastern North China craton reveal dramatic variations of up to 6% differences in shear wave velocity, with some of the lowest velocities existing in the upper mantle beneath the Trans-North China Orogen (Fig 10c). Densities in the upper mantle at these locations, as calculated by FWEA18, also reveal a dramatic difference between the western and the central and eastern portions of the NCC (Fig 10d). The inversion results of the FWEA18 model in the North China Craton lithosphere and upper mantle are consistent with previous regional tomographic models of the mantle, including those of Tian et al. (2009), Zheng et al. (2011), and Lei (2012).

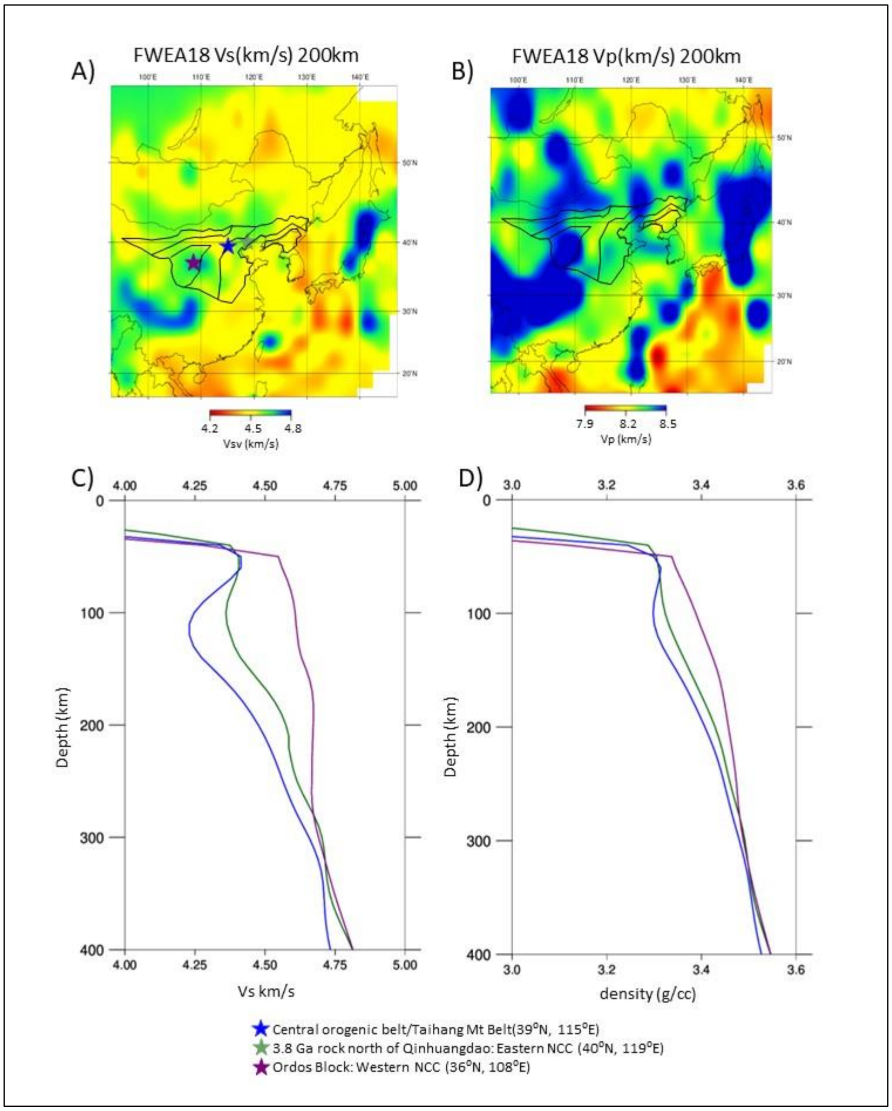

Figure 10. Depth slices and 1D S-velocity models through the FWEA18 tomographic model (Tao et al., 2018) highlighting variations in the North China Craton. (**a**) S-velocity depth slice at 200 km; (**b**) P-velocity depth slice at 200 km, (**c**) 1D S-velocity model to 400 km depth at locations marked in (**a**), (**d**) density model from the FWEA18 tomographic inversion at these locations.

7.2.2. Wyoming craton

The Wyoming craton has a history extending back to the Eoarchean, and Hf isotopic compositions of 3.8 Ga zircon suggest Hadean origins (Mueller et al., 1998; Frost et al., 2017). Like the Zimbabwe craton, the northern and central portions of the Wyoming craton are characterized by high μ that requires Eoarchean differentiation and formation of an isotopically evolved reservoir (Wooden & Mueller, 1988; Frost et al., 1998). The craton is composed of three sub-provinces, all of which amalgamated by 2.62 Ga (Mueller & Frost, 2006)(Fig. 9b). The Montana Metasedimentary Terrane and Bighorn-Beartooth Magmatic Zone sub-provinces are characterized by the presence of a high velocity lower crustal “7.xx” layer that is not present in the Southern Accreted Terranes sub-province (Gorman et al., 2002; Snelson et al., 1998) (Fig.

11a). The latter is interpreted as a collage of juvenile and older blocks accreted to the rest of province at 2.62 Ga (Frost et al., 2006). The province has experienced no penetrative

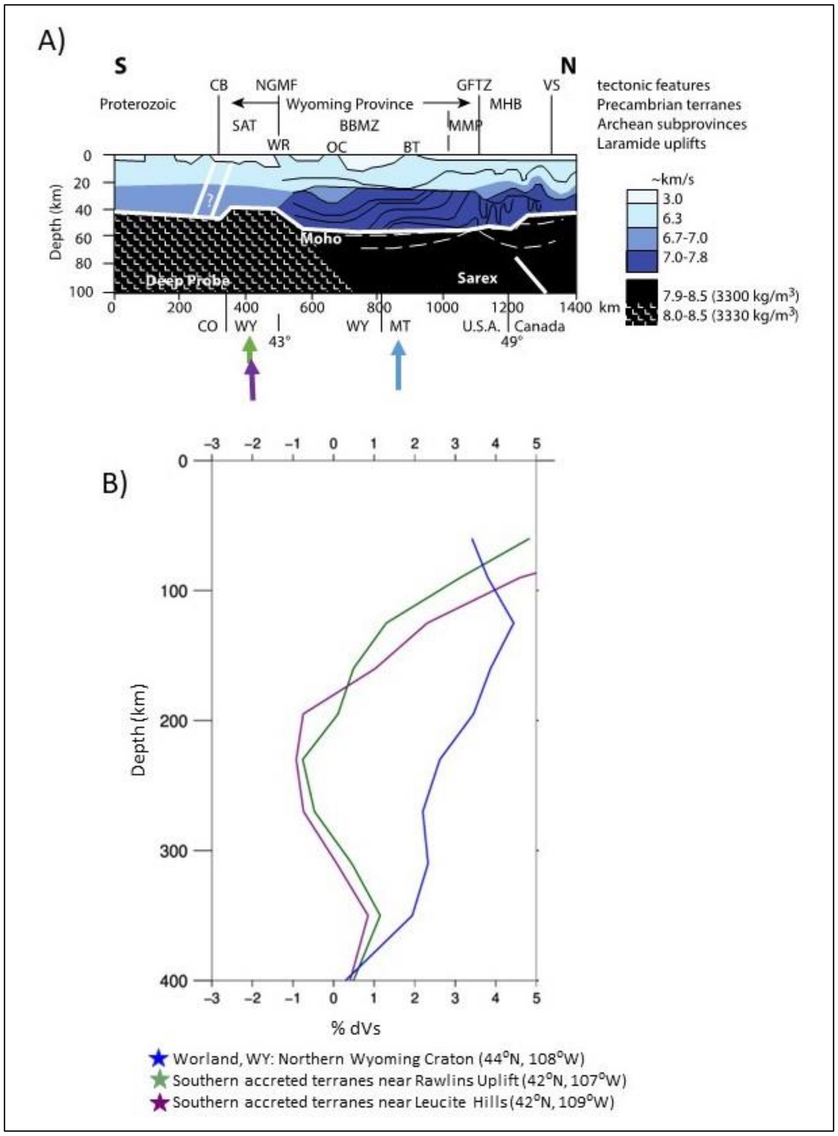

Figure 11. (**a**) Interpreted velocity model for the Wyoming craton crust and upper mantle from Deep Probe and Sarex experiments (Gorman et al., 2002; Snelson et al, 1998), showing the fast "7.xx" layer beneath the northern Wyoming province. CB = Cheyenne belt; NGMF = North Granite Mt. fault; GFTZ = Great Falls Tectonic Zone; MHB = Medicine Hat block; SAT = Southern Accreted Terranes; BBMZ = Beartooth-Bighorn Magmatic Zone; MMP = Montana Metasedimentary Province; WR = Wind River Mts.; OC = Owl Creek Mts.; BT = Beartooth Mountains, (**b**) 1D models of S-velocity variations (%dVs) through the regional WUS model by Schmandt and Humphreys (2010) at three locations in the Wyoming craton indicated by colored arrows in (**a**).

deformation since 2.50 Ga (Mueller & Frost, 2006).

The Wyoming craton is surrounded by Proterozoic orogens on the north (Great Falls Tectonic Zone), east (Dakota/Trans-Hudson Orogen), south (Cheyenne belt), and west (Farmington zone)(Fig. 9b). It was intruded by the mafic Stillwater Complex at 2.70 Ga, and by Proterozoic mafic dikes. The craton has been variably affected by the Sevier and Laramide orogenies, both related to shallow subduction of the Farallon plate (Grand, 1994), and by Eocene felsic magmatism related to its removal (Humphreys, 1995; Feeley, 2003). Today the craton is impinged on the northwest by the Yellowstone hotspot, and on the south by the Rio Grande rift. Xenoliths from Williams and Homestead areas in MT were metasomatized during the Laramide (Carlson et al., 2004). Thus, there are many post-Archean events that may have affected and potentially weakened the subcratonic mantle lithosphere.

The Wyoming craton is perhaps one of the best studied Archean cratons, geophysically (Dave & Li., 2016; Chai et al., 2015; Porritt et al., 2014; Schmandt & Humphreys, 2010; Yuan & Dueker, 2005). Its accessibility for instrumentation together with the seismicity of the western United States has enabled extensive data collection. Many regional- and local-scale tomographic models have been created that cover the region of the Wyoming craton (Dave & Li., 2016; Chai et al., 2015; Porritt et al., 2014; Yuan & Dueker, 2005), with one of the most robust being the WUS model by Schmandt and Humphreys (2010). As noted above, a comparison of the dVs global tomographic model, Sglobe_rani and WUS (Fig. 5) shows that well established features, such as the Yellowstone hotspot, are not resolved by the global model but a number of geologic features correlate with fast and slow regions on the regional tomographic model. The Yellowstone hotspot track is marked by a prominent area of seismically slow lithosphere trending NE-SW across Idaho and impinging on the Wyoming craton in the vicinity of Yellowstone Park. On the west, the Basin and Range province is associated with slow velocities at all depths. Also discernible as a zone of slow velocities is the Rio Grande Rift, which trends N-S through New Mexico and Colorado, terminating near the Wyoming-Colorado state line. Finally, a clear difference in S-velocities between the northern and southern portions of the craton are especially apparent from 150 to 250 km depth (Fig. 5b). The thinner cratonic lithosphere beneath the southernmost portion of the Wyoming craton is observed in other regional models of the western United States, including model DNA13 (Porritt et al., 2014; Dave & Li, 2016).

Three 1D %dVs depth profiles were constructed using the Schmandt and Humphreys (2010) model (Fig. 11b). The blue profile is located within the older, northern portion of the Wyoming craton, whereas the purple and green curves are located in the younger, southern part. The northern profile exhibits the fast S-velocities typical of cratonic lithosphere. It does not show effects of Laramide-age metasomatism identified in kimberlite xenoliths erupted through the Wyoming craton farther north in central Montana (Carlson et al. (2004). In contrast, both southern profiles indicate that in this region the craton lacks a fast, thick cratonic keel. These southern profiles lie within the Southern Accreted Terranes, where the Wyoming craton appears to lack fast lower crust (Gorman et al., 2002; Snelson et al., 1998)(Fig. 11a). The correlation between crustal structure and mantle velocity structure raises the question whether the Southern Accreted Terrane lost its fast lower crust and mantle root, or if it never had a fast lower crust. Current data and observations do not distinguish between these alternatives.

7.2.3. Madagascar craton

The Madagascar craton is composed of an ancient central nucleus of gneisses, 3.3 to 3.1 Ga, surrounded by supracrustal suites and younger mostly juvenile granitoids (2.70-2.56 Ga). The juvenile rocks were accreted to the old gneisses, then metamorphosed and intruded by granitoids at ~2.5 Ga, forming the Madagascar craton (Tucker et al., 2014; Fig. 9c). Similarities to Archean rocks in India suggest that the Madagascar craton was part of the Greater Dharwar craton until the Early Cretaceous dispersal of Gondwana (Reeves, 2014).

The Archean rocks of the Madagascar craton have been extensively reworked by a number of Proterozoic and Phanerozoic events. Paleoproterozoic mafic magmatism in the northern part of the craton may indicate a period of rifting that partially disrupted the craton. This event was followed by accretion of a Paleoproterozoic terrane composed of 2.2-1.8 Ga gneisses in south Madagascar (Tucker et al., 2014). During the Mesoproterozoic, sequences of platform sediments were deposited upon the Archean craton and surrounding Paleoproterozoic crust. In the early Neoproterozoic, a juvenile magmatic arc of calc-alkaline intrusive rocks and related volcano-sedimentary strata were built upon the edge of the Archean shield, requiring a prior rifting event between the Archean core and accreted Paleoproterozoic crust. The most intense period of deformation and magmatism occurred in late Neoproterozoic time, during oblique convergence of East and West Gondwana. A bimodal intrusive suite of dikes and sills and small intrusive bodies was emplaced across a broad area at the same time that elongate basins filled with Neoproterozoic sediment. Tucker et al. (2014) interpret this event as consistent with continental dilation related to plume-induced melting or crustal delamination and asthenospheric upwelling. This was followed by Pan-African metamorphism, deformation, and intrusion of syn- and post-tectonic granites. During the dispersal of Gondwana, Madagascar first rifted from Africa during the opening of the Somali Ocean, then separated from India when the

Marion plume became active (ca 88 m.y.), dikes and basalt flows were emplaced in southern and eastern Madagascar, and India moved rapidly to the northeast (Reeves, 2014).

Although Madagascar is on the edge of Africa.ENT coverage, the current regional tomographic models are not at the resolution to adequately image the craton. In this region of Africa.ENT, checkerboard resolution tests provided by Emry et al. (2018) suggest that the amplitude of features should be accurate, although weaker, and that some directional smear in the NW-SE direction is present due to the geometrical limitations of source-receiver pairs. With this caveat, the slight green color at 210 and 260 km from the Africa.ENT model reveals that the Archean Madagascar craton is seismically faster than model upper mantle, if less fast than Archean cratonic lithosphere in adjacent Africa (Fig. 8ab). A 1D profile constructed using the global model CAM2016 suggests that the Madagascar mantle lithosphere does not have the fast

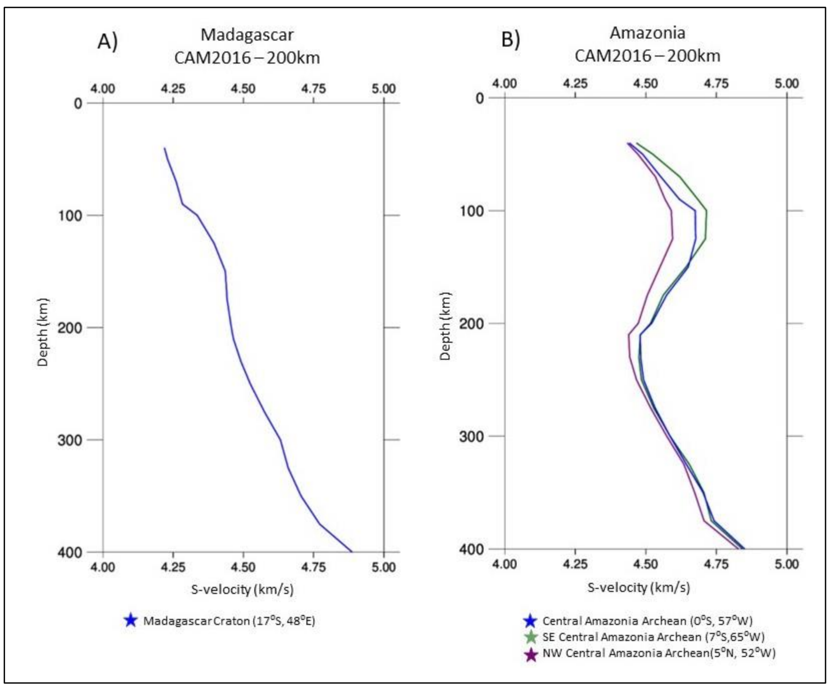

Figure 12. 1D S-velocity profiles for Madagascar and Amazonia constructed using the CAM2016 global tomography model (Priestley et al., 2019). (**a**) Madagascar profile, location shown on Fig. 8A. (**b**) 1D profiles for Amazonia. Locations of profiles are shown on Fig. 13.

seismic velocities of stable cratons, and thus likely has been modified (Fig. 12a).

7.2.4. Amazonian craton

Unlike the Yilgarn, Zimbabwe, Wyoming and North China cratons, the Amazonian craton has no known Eoarchean/Hadean history (Silva-Sliva et al., 2020). The craton includes three areas of Archean crust of Meso- and Neoarchean age known as the Central Amazonian Province, surrounded by NW-SE trending belts of Proterozoic crust added at 2.25-2.05, 1.98-

1.81, 1.78-1.55, and 1.28-0.95 Ga (Fig. 13) (Cordani et al., 2009). On the west, the craton is bordered by the Sunsas Belt, formed during Mesoproterozoic and interpreted as the southern

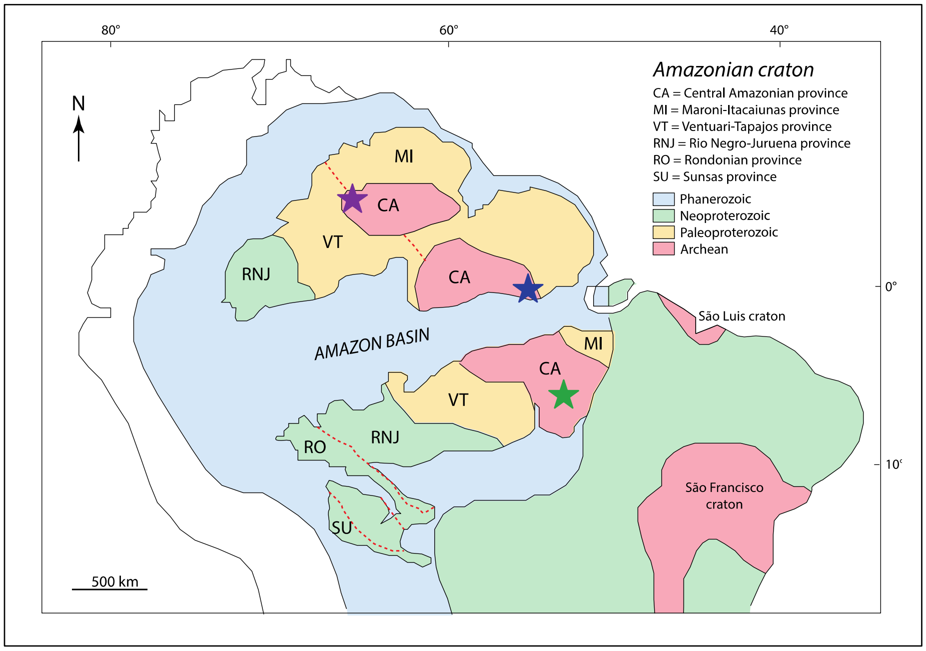

Figure 13. The Central Amazonian Province is comprised of three areas of Archean rocks. Most of the Amazonian craton is Proterozoic in age. Craton boundaries from Cordani et al. (2009).

extension of the Grenville Orogeny of North America (Santos et al., 2008)). The east-west trending Amazon basin in the central part of the craton represents a 550 Ma rift (Cordani et al., 2009). The Nazca subducted slab extends beneath the craton today at depths of ~800-1000 km, as imaged by Portner et al. (2019).

Few regional tomographic models exist in South America that adequately cover the Archean portion of the Amazonian craton to mid-mantle depths. Feng et al.’s (2007) model clearly images the fast velocity signature of the Brazilian craton above 200 km but does not have adequate resolution below 200 km depth to decipher the current state of the cratonic root. Portner et al.’s (2020) model focuses on the Nazca slab and the deeper mantle and has model gaps in our area of interest. Ambient noise tomography has also been attempted in the South American craton, but not in the region of the Archean Amazonian craton (Goutorbe et al., 2015). An upper mantle model beneath the southern Atlantic Ocean, South America and Africa, does reveal a cratonic root extending to at least 220 km depth beneath the Amazonian craton in their Vs model (Celli et al., 2020a), including beneath the Amazonian basin rift. The Proterozoic areas west of the Archean Amazonian craton exhibits slower velocities than to the east. Celli et al. (2020a) propose either that the western Proterozoic portion of Amazonia never developed a thick lithospheric root, or that it has been removed. If the latter, they suggest that metasomatism or deformation and reworking during the Mesoproterozoic Sunsás orogeny could be responsible. Figure 12 provides 1D profiles of the three Archean areas of the Amazonian craton, as imaged using the global tomographic models CAM2016. These profiles show the fast S-velocities and inflection at ~200 km characteristic of cratons. The northwestern profile suggests slightly slower S-velocities under this part of Amazonia, but none of the profiles indicates significant modification of Amazonian cratonic lithosphere.

8 Discussion

8.1 Comparison of case study cratons using CAM2016 global model

As described above, regional models reveal relatively detailed tomographic images and profiles beneath individual cratons, but because of different theoretical assumptions, parameterization, and data used they cannot be compared directly. For this reason, we have used the CAM2016 global velocity model to compare 1D depth-velocity models for each of the cratons (Fig. 14). Multiple profiles from each craton, representing the different larger provinces in various geographic locations, were averaged to produce a composite profile (Appendix 1). To illustrate the distinct lithospheric velocity structures of unmodified or variably modified areas

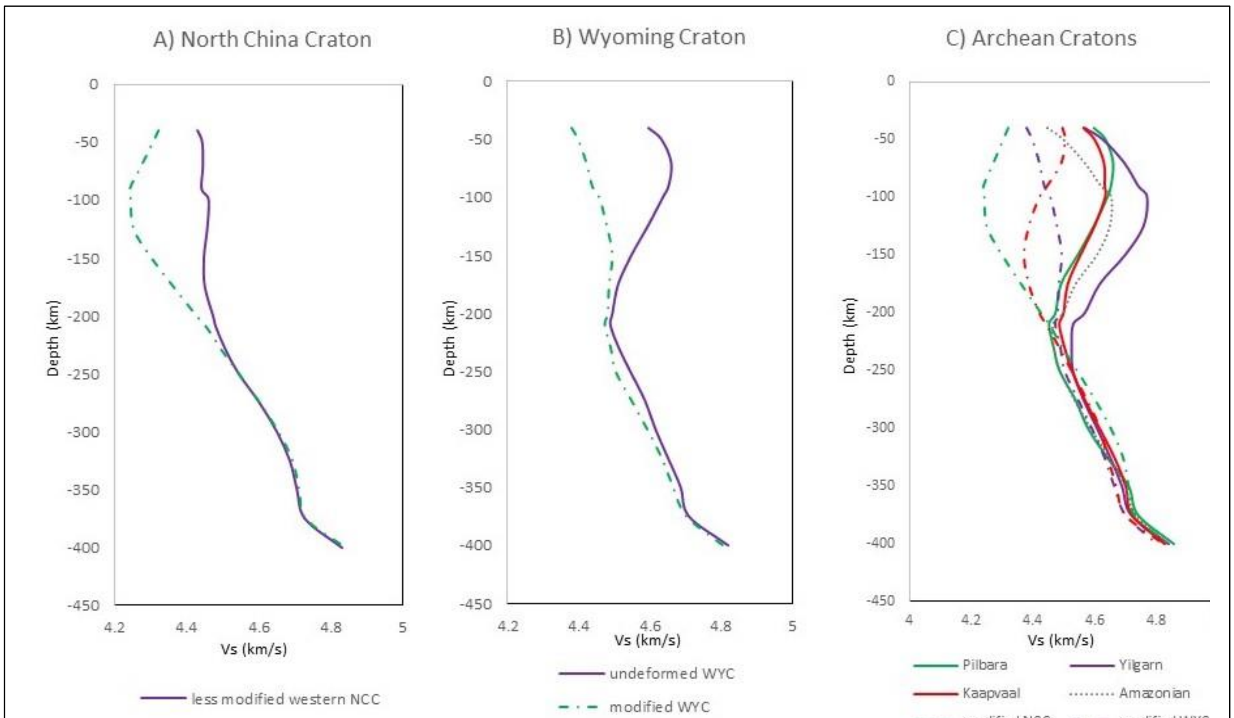

Figure 14. Comparison of 1D upper mantle S-velocity profiles for case study cratons, using global tomographic model CAM2016 (Priestly et al., 2019). (**a**) average 1D models through the modified and unmodified portions of the North China craton; (**b**) average 1D models through the modified and unmodified regions of the Wyoming craton; (**c**) average 1D profiles through other modified and unmodified cratons.

within the North China and Wyoming cratons, two composite profiles were developed for each of these cratons. Neither profile from the North China craton (Fig. 14a) shows the high S-velocities of unmodified cratonic lithosphere. However, the lithosphere beneath the eastern block has been more strongly affected by modification than the western block. The northern Wyoming craton, by contrast, preserves the fast S-velocities within its 200 km cratonic keel (Fig. 14b), but the lithosphere beneath the southern part of the craton is slower and resembles the near-vertical, global average profile of approximately 4.5 km/s (c.f. Fig. 6).

1D profiles of the unmodified cratons, Pilbara, Yilgarn, Kaapvaal, and Zimbabwe, are shown by solid lines in Fig. 14c. These show the characteristic fast S-velocities within the top 200 km of the lithosphere and an inflection in velocity at approximately 200 km, at the base of the cratonic keel. The contrasting profiles for the modified portions of North China and Wyoming, and for Madagascar, are shown in dot-dash patterns on Fig. 14c. These reveal slower velocities within the top 200 km, with shapes that vary from near vertical to convex. The CAM2016 model images a profile for the Archean Amazonian craton that is similar to the profiles for these unmodified cratons (dotted profile in Fig. 14c). Although it has been interpreted as modified (Kusky et al., 2014), Amazonia exhibits the characteristic fast S-velocity structure in the upper 200 km beneath the Central Amazonian province, suggesting that the craton has retained its stability.

Table 3 summarizes the tomographic characteristics and the geologic and tectonic histories of the cratons reviewed in this study. Some of those with strong cratonic lithosphere, such as Pilbara and Yilgarn, have avoided later tectonism that could potentially modify and destroy cratonic keels. Others in this group, including Kaapvaal, Zimbabwe, and Amazonia, have been exposed to potentially destabilizing tectonic processes, yet at the scale of global and regional tomographic models, they appear to retain strong cratonic keels. As discussed above, tomographic imaging of North China, Wyoming, and Madagascar suggests that these cratons lack strong cratonic lithosphere, either wholly or in part. What makes some cratons susceptible to destruction, whereas others appear to survive?

8.2 Nature: characteristics of stable cratons

Three geodynamical properties provide clues to the characteristics of stable cratons (Table 1): (1) buoyant, thick lithosphere formed by extraction of high-fraction partial melts early in Earth history when mantle temperatures were higher, (2) an increasingly viscous lithosphere formed by cooling of fluid-, melt-, and heat-producing element-depleted cratonic lithosphere subsequent to cratonization, and (3) comparatively high integrated yield strength of equant cratonic blocks that minimize margins exposed to tectonism and focus deformation within younger orogenic "crumple zones" (Lenardic et al., 2000). The summary table for our case study cratons (Table 3), indicates that the stable Australian and southern African cratons meet these requirements: all have histories extending back to the Paleoarchean, were assembled in the Archean. Zimbabwe and Kaapvaal were amalgamated along the Limpopo belt during the Neoarchean, and Yilgarn and Pilbara were joined along the Capricorn orogen at 2 Ga. Both of these composite cratons were then enveloped in younger, Proterozoic orogens that potentially could insulate them from tectonism. Although Amazonia has no known pre-Mesoarchean history, the Archean craton is large and surrounded by younger Proterozoic belts, features that may predispose it, too, to long-term stability.

The three cratons that do not preserve cratonic lithosphere, either in full or in part, also have geologic histories extending back at least as far as the Paleoarchean. They vary in size, with Madagascar left the smallest after it rifted from the Dhawar craton during break-up of Gondwana. Like the stable cratons described above, they are built from Archean blocks of various ages, including in the case of Wyoming a southern subprovince composed of juvenile Neoarchean terranes. Madagascar and Wyoming both were cratonized by the end of the Archean. The North China craton was assembled later: four Archean blocks were joined at 2.0-1.9 Ga to form the largest of the cratons we studied. All are surrounded by younger orogens. There is no definitive evidence to indicate that any of these Archean cratons were by nature destined for destruction.

Table 3
Major characteristics and tectonic processes that could affect stability of cratons

Archean craton	**Global and Regional Tomography**	**Nature: born strong?**	**Nurture: destabilizing processes?**	**Summary**
Stable cratons with strong cratonic lithosphere				
Pilbara and Yilgarn	Cratonic profiles	Old: $\geq$Paleoarchean histories Size: small (0.18 x 10^6 km^2) to moderate (0.6 x 10^6 km^2) Archean craton assembly:	Located in plate interiors since Paleoproterozoic	Stable, not subject to post-Archean tectonism

		3.0 Ga and 2.63 Ga respectively Yilgarn & Pilbara were joined at 2 Ga along Capricorn orogen, then to more extensive Australian continent		
Zimbabwe and Kaapvaal	Cratonic profiles	Old: Meso- and Paleoarchean crust; Zimbabwe has Pb isotopic evidence of early crust Size: small (0.24 x 10^6 km^2) to moderate (0.55 x 10^6 km^2) Zimbabwe and Kaapvaal were joined along Limpopo belt at 2.7-2.65 Ga Proterozoic additions to 1.0 Ga formed Kalahari craton, doubling size	Xenolith evidence of melt or fluid Si-metasomatism during amalgamation of Kaapvaal Bushveld intruded at 2.06 Ga in northern Kaapvaal craton Mesozoic Karoo magmatism, kimberlite eruption	Modification is insufficient to destablilize Archean areas
Amazonia	Cratonic profile	Young: No pre-Mesoarchean history, Meso- and Neoarchean crust in Central Amazonian province Size: large (~1.2 x 10^6 km^2) Belts of Proterozoic crust added between 2.25 and 0.95 Ma	Amazon basin represents a 550 Ma rift Nazca flat-slab subduction	Cratonic keel remains beneath Archean areas
Cratons lacking (wholly or in part) strong cratonic lithosphere				
North China	Variably modified	Old: Paleoarchean rocks, Eoarchean zircon, Pb isotope evidence for old crust in eastern block Size: large (1.5 x 10^6 km^2) composite of four Archean blocks amalgamated at 2.0-1.9 Ga Surrounded by Proterozoic orogens	Paleozoic basin subsidence suggests possible refertilization of lower cratonic mantle lithosphere Mesozoic flat-slab subduction, magmatism	Keel has been modified, esp. in eastern block
Wyoming	Cratonic profile is absent in south	Old: Paleoarchean crust, Eoarchean zircon, Pb isotopic evidence of early crust in north Size: moderate (0.45 x 10^6	Farallon flat subduction, Sevier & Laramide orogenies 80-35 Ma Yellowstone hotspot, Rio Grande rift	Northern Wyoming remains stable, cratonic keel is absent in south

		km^2) Last magmatism, alteration at 2.55 Ga Surrounded by Proterozoic orogens		
Madagascar	Modified	Old: Paleoarchean gneiss core Size: small (0.25 x 10^6 km^2) (rifted portion of Dhawar craton) Craton amalgamated at ~2.5 Ga	Paleoproterozoic mafic magmatism and rifting in north Neoproterozoic magmatic arc Late Neoproterozoic bimodal magmatism followed by Pan-African metamorphism, deformation, magmatism, Gondwana dispersal	Cratonic keel has been destroyed

8.3 Nurture: modification does not necessarily result in instability and destruction

Tectonic and magmatic events that affected the cratons examined in our study include plume activity, rifting, flat-slab subduction, and associated magmatism. Examination of Table 3 reveals one mechanism that predisposes cratons for stability: locations in plate interiors where many destructive tectonomagmatic processes may be avoided. Pilbara and Yilgarn have not been located along plate margins since the Paleoproterozoic and thus have escaped modification by heat and metasomatizing fluids and melts associated with subduction. Plume activity also does not seem fatal to cratonic lithosphere. The Bushveld intrusion formed at 2.1 Ga in the northern Kaapvaal craton and the Yellowstone hotspot is currently impinging on northwestern Wyoming. Although the lithosphere has slower velocity under Bushveld than elsewhere in Kaapvaal and Zimbabwe (Youssof et al., 2015), and the mantle below the Yellowstone hotspot track likewise is associated with slower velocities (see Fig. 10) the presence of plume-related magmatism does not seem to be associated with wholesale loss of cratonic lithosphere. Mantle plumes appear to have eroded Proterozoic portions of the Kalahari craton, but do not appear to have affected the Archean cratonic mantle (Celli et al., 2020b). Rifting likewise may be an ineffective process for destroying cratonic lithosphere. The Central Amazonian mantle lithosphere appears continuous beneath the Amazonian Basin rift (Celli et al., 2020a), and the Rio Grande Rift has not penetrated the Wyoming craton, at least to date.

Metasomatism appears to be the most effective process for modifying and potentially destroying cratonic mantle. Metasomatism associated with subduction and rollback is most likely responsible for the delamination and loss of cratonic lithosphere beneath the North China craton (e.g., Kusky et al., 2014; Liu et al., 2019) and also has been cited for destruction of the Wyoming cratonic keel (Carlson et al., 2004; Kusky et al., 2014). Evidence of metasomatism is present in mantle xenoliths from both cratons, although the North China mantle lithosphere is more thoroughly destroyed. Flat-slab subduction is taking place beneath Amazonia today (Portner et al. 2019), but it lies at great depth does not yet appear to have affected the strength of Archean cratonic lithosphere.

There is some evidence to suggest that metasomatism primarily affects the base of the cratonic lithosphere. Mantle xenoliths from greater depth tend to be more fertile and metasomatized than the more highly melt-depleted peridotitic xenoliths from shallower levels (Lee et al., 2011; Griffin et al., 2003). These studies interpreted geochemical and isotopic data from the deeper xenoliths to suggest that the lower cratonic lithosphere was refertilized by metasomatism, rather than representing undepleted mantle, a process that may destabilize the deeper cratonic lithosphere and make it susceptible to removal by mantle flow.

The extent and rate of metasomatism is likely to vary. As Carlson et al. (2005) observed, metasomatism localized in veins is unlikely to affect the average composition and stability of the lithosphere. If the metasomatism is widespread and infiltrates broad areas, then the effects could be more consequential. It could be a cumulative process that affects cratonic lithosphere over a long period of time, as described by Liu et al. (2019) for the North China craton, who describe two prolonged episodes of subsidence that they related to infiltration of metasomatizing melts into the lower cratonic mantle. Or metasomatism may be associated with a discrete event, such as shallow subduction of the Farallon slab followed by rollback and asthenospheric upwelling beneath the Wyoming craton (Feeley, 2003; Carlson et al., 2004).

Metasomatized cratonic lithosphere is not necessarily destined for destruction. Mantle xenoliths from Kaapvaal provide evidence of Si-metasomatism, yet the craton remains stable. Perhaps a future, major tectonic event may cause the metasomatized lithosphere to founder. Or perhaps metasomatism affects buoyancy and integrated yield strength sufficiently to set a craton on a course for eventual destruction. To investigate these questions, we return to stability regime diagrams.

8.4. Effects of modification on craton stability

The velocity differences between stable and modified cratonic lithosphere are small—less than 10%. Likely not all of that velocity difference is due to composition, but some certainly is connected to compositional change, which would in turn affect the buoyancy of the cratonic lithosphere. We can quantify the amount of change in the relative buoyancy of cratonic lithosphere potentially associated with metasomatism assuming that it would result in a decrease in Mg#, which in turn will be reflected in a decrease in the observed seismic velocity. For example, Lee (2003) determined that a 1% change in s-wave velocity can be attributed to a five-unit change in the Mg#. Assuming Mg# values typical of cratonic lithosphere, 92-93 (Lee et al., 2011), a five unit decrease in Mg# would move it closer to values indicative of fertile mantle (~88, Lee et al., 2011). Effect of this change in Mg# on cratonic lithospheric mantle density can be estimated using the empirical relationship of Lee (2003). This change in density can then be transferred into the equation for buoyancy ratio (e.g., Cooper et al., 2006; $B = \frac{\Delta\rho}{\rho_m \alpha \Delta T}$, where $\Delta\rho$ is the density difference between the cratonic lithosphere (including both the crust and mantle) and mantle, ρ_m is the mantle density, α is the coefficient of thermal expansion, ΔT is the temperature difference across the upper mantle). Using average values for thermal expansion ($3x10^{-5}$ °C^{-1}), mantle density (3.3 g/m^3), and temperature difference across the upper mantle (1400 °C), and assuming that the cratonic mantle lithosphere contributes to 70% of the overall average lithospheric density, then the change in buoyancy associated with this magnitude of change in Mg# can lower the values of the buoyancy ratio by ~0.4 units. Depending on lithospheric thickness and original compositions, this reduction in buoyancy is sufficient to move a craton into a different stability condition, resulting in the potential for deformation. For example, if the starting buoyancy ratio of the cratonic lithosphere was 1.0 (a likely value for cratonic mantle lithosphere with a Mg# of 91), then a reduction of the buoyancy ratio of 0.4 units dramatically narrows the range of Rayleigh numbers over which the craton is stable, affecting its longevity (Fig. 3). However, if the starting buoyancy ratio was closer to 1.5, then the reduction of the buoyancy ratio of 0.4 units does not result in as much of a reduction of longevity. This sensitivity suggests that although metasomatism may be an important process in modifying cratons, its effect on cratonic lithosphere will depend upon the initial state of the cratonic lithosphere as well as on the magnitude of metasomatism. The potential for destruction could be further exacerbated if the metasomatism also lowers the viscosity and/or contributes to thinning of the cratonic lithosphere, as both are confounding factors in craton stability.

9 Conclusions: Nature or nurture? Lessons on craton stability

This study integrates geodynamic, geological, and geophysical perspectives and data in order to evaluate the relative importance of *nature*—the initial conditions of a craton—versus *nurture*—the subsequent tectonic processes that may modify and destabilize cratonic lithosphere. Our review of eight cratons suggests that continental lithosphere formed and cratonized prior to the end of the Archean has the potential to withstand subsequent deformation, heat, and metasomatism.

Some of the cratons with present-day 1D tomographic profiles indicative of stability have survived by avoiding destabilizing tectonic processes, or have been shielded by surrounding Proterozoic "crumple zones", or both. Processes that enable metasomatism of the cratonic lithosphere appear to be the most destabilizing because metasomatism affects buoyancy, viscosity, and integrated yield strength. The volume and geometry of mantle lithosphere affected by metasomatism is likely to be critical: local networks of metasomatized veins associated with kimberlite emplacement will be less destabilizing than wholesale metasomatism of the lower cratonic mantle or metasomatism that produces a weak plane along which delamination could occur.

Stability regime diagrams are a reminder that craton stability is a function not only of the extent and geometry of modification, but also of time. Because stability changes as the Earth cools, cratons that are marginally stable today may pass into conditions of marginal instability in the future, and even mild deformational stresses could trigger destruction.

In summary, cratons born strong are not guaranteed survival. Both nature and nurture factor into craton stability and longevity, and there are multiple pathways to craton destruction.

Appendix 1
Locations of 1D tomographic profiles combined to produce composite cratonic profiles shown on Figure 14

Craton	Latitude	Longitude
Pilbara	-20	-20
	-19.8	-19.8
	-20	-20
	-20.2	-20.2

Yilgarn	-26 -25 -32 -28	120 118 118 124
Kaapvaal and Zimbabwe Zimbabwe Limpopo N Kaapvaal S Kaapvaal	 -17 -20 -23 -27	 29 28 23 28
E North China (more modified)	45 39 35 33	125 127 117 116
W North China (less modified)	39 38 36 37	103 105 110 110
Madagascar	-16 -17 -18 -20	48 47 46 47
Amazonia	4 0 0 -5	-65 -60 -57 -54
N Wyoming (unmodified)	47 45 47 46	-107 -105 -104 -105
S Wyoming (modified)	43 45 42 45	-107 -109 -110 -111

Acknowledgments, Samples, and Data

This paper is the outgrowth of an EarthScope synthesis workshop held in January 2019 in Bozeman, Montana. The authors acknowledge travel support to the workshop from the EarthScope National Office. We also acknowledge IRIS DMC for tomographic mapping (Trabant et al., 2012). All tomographic models are publicly available through the IRIS data respository.

References

Abt, D.L., Fischer, K.M., French, S.W., Ford, H.A., Yuan, H., & Romanowicz, B. (2010). North American lithospheric discontinuity structure imaged by *Ps* and *Sp* receiver functions. *Journal of Geophysical Research*, 115, B09301.https://doi.org/10.1029/2009JB006914

Aulbach, S., Massuyear, M., & Gaillard, F. (2017). Origins of cratonic mantle discontinuities: a view from petrology, geochemistry and thermodynamic models. *Lithos*, 268-271, 364-382.

Beall, A.P., Moresi, L., & Cooper, C.M. (2018). Formation of cratonic lithosphere during initiation of plate tectonics. *Geology*, 46, 487-490.

Berger, M., & Rollinson, H. (1997). Isotopic and geochemical evidence for crust-mantle interaction during late Archaean crustal growth. *Geochimica et Cosmochimica Acta*, 61, 4809-4829.

Best, M.G., & Christiansen, E.H. (1991). Limited extension during peak Tertiary volcanism, Great Basin of Nevada and Utah. *Journal of Geophysical Research*, 96, 13,509-13,528.

Byerlee, J. (1968). The brittle-ductile transition in rocks. *Journal of Geophysical Research*, 74, 4741-4750.

Carlson, R.W., Pearson, D.G., Boyd, F.R., Shirey, S.B., Irvine, G., Menzies, A.H., & Gurney, J.J. (1999). Re-Os systematics of lithospheric peridotites: implications for lithosphere formation and preservation. Cape Town, South Africa, 7th International Kimberlite Conference Proceedings, p. 99-108.

Carlson, R.W., Irving, A.J., Schulze, D.J., & Hearn, B.C. (2004). Timing of Precambrian melt depletion and refertilization events in the lithospheric mantle of the Wyoming Craton and adjacent Central Plains Orogen. *Lithos*, 77, 453-472.

Carlson, R.W., Pearson, D.G., & James, D.E. (2005). Physical, chemical, and chronological characteristics of continental mantle. *Reviews of Geophysics*, 43, RG1001, https://doi.org/10.1029/2004RG000156

Cassel, EJ, Smith, ME, & Jicha, B. (2018). The impact of slab rollback on Earth's surface: uplift and extension in the hinterland of the North American Cordillera. *Geophysical Research Letters*, 45, 10,996-11,004.

Cawood, P.A., & Korsch, R.J. (2008,). Assembling Australia: Proterozoic building of a continent. *Precambrian Research*, 166, 1-38.

Celli., N.L., Lebedev., S., Schaeffer, A.J., Ravenna., M., & Gaina., C. (2020a). 1. The upper mantle beneath the South Atlantic Ocean, South America and Africa from waveform tomography with massive data sets. *Geophysical Journal International*, 22, 178-204.

Celli, N.L., Lebedev, S., Schaeffer, A.J., & Gaina, C. (2020b). African cratonic lithosphere carved by mantle plumes. *Nature Communications*, 11-92. https://doi.org/10.1038/s41467-019-13871-2

Chai, C., Ammon, C.J., Maceira, M., & Herrmann, R.B. (2015). Inverting interpolated receiver functions with surface wave dispersion and gravity: Application to the western U.S. and adjacent Canada and Mexico. *Geophysical Research Letters*, 42, 4359-4366. https://doi.org/10.1002/2015GL063733

Chang, S.-J., Ferreira, A.M.G., Ritsema, J., van Heijst, H.J., & Woodhouse, J.H. (2015). Joint inversion for global isotropic and radially anisotropic mantle structure including crustal thickness perturbations. *Journal of Geophysical Research*, 120, 4278-4300. https://doi.org/10.1002/2014JB011824

Chapin, C.E. & Cather, S.M. (1994). Tectonic setting of the axial basins of the northern and central Rio Grande rift. In Keller, GR & Cather, SM, (Eds.), *Basins of the Rio Grande Rift: structure, stratigraphy, and tectonic setting*. Geological Society of America Special Paper (Vol. 291, pp. 5-25) Boulder, CO: Geological Society of America.

Chu Z-Y, Wu F-Y, Walker RJ, Rudnick, R.L., Pitcher, L., Puchtel, I.S., Yang, Y.-H., & Wilde, S.A. (2009). Temporal evolution of the lithospheric mantle beneath the Eastern North China Craton. *Journal of Petrology*, 50, 1857–1859.

Conrad, C.P., & Molnar, P. (1999). Convective instability of a boundary layer with temperature- and strain-rate-dependent viscosity in terms of “available buoyancy.” *Geophysical Journal International*, 139, 51–68.

Conrad, C.P., & Lithgow-Bertelloni, C. (2006). Influence of continental roots and asthenosphere on plate-mantle coupling. *Geophysical Research Letters*, 33, doi.org/10.1029/2005GL025621

Cooper, C. M., & Miller, M. S. (2014). Craton formation: Internal structure inherited from closing of the early oceans. *Lithosphere*, 6, 35-42.

Cooper, C.M., & Conrad, C.P. (2009). Does the mantle control the maximum thickness of cratons? *Lithosphere*, 1, 67–72.

Cooper, C.M., Lenardic, A., & Moresi, L. (2004). The thermal structure of stable continental lithosphere within a dynamic mantle. *Earth and Planetary Science Letters*, 222, 807-817.

Cooper, C.M., Lenardic, A., Levander, A., & Moresi, L. (2006) Creation and preservation of cratonic lithosphere: seismic constraints and geodynamic models. In Benn, K., Mareschal, J.-C., and Condie, K.C. (Eds.), *Archean geodynamics and environments*, Geophysical Monograph Series (Vol. 164, pp. 75-88). Washington, DC: American Geophysical Union.

Cooper, C.M., Miller, M.S., & Moresi, L. (2017). The structural evolution of the deep continental lithosphere. *Tectonophysics*, 695, 100-121.

Cordani, U.G., Teixeira, W., D'Agrella-Filho, M.S., & Trindade, R.I. (2009). The position of the Amazonian Craton in supercontinents. *Gondwana Research*, 15, 396-407.

Cottrell, E., Jaupart, C., & Molnar, P. (2004). Marginal stability of thick continental lithosphere. *Geophysical Research Letters*, 31, L18612. https://doi.org/10.1029/2004GL020332

Currie, C.A., & van Wijk, J. (2016). How craton margins are preserved: Insights from geodynamic models. *Journal of Geodynamics*, 100, 144–158.

Dave, R., & Li, A. (2016). Destruction of the Wyoming craton: seismic evidence and geodynamic processes. *Geology*, 44, 883-886.

Davies, G.F. (1994). Thermomechanical erosion of the lithosphere by mantle plumes. *Journal of Geophysical Research*, 99, 15,709-15,722.

Dziewonski, A.M., & Anderson, D.L. (1981). Preliminary reference Earth model. *Physics of the Earth and Planetary Interiors*, 25, 297-356.

Duffy, T.S., & Anderson, D.L. (1989). Seismic velocities in mantle minerals and the mineralogy of the upper mantle. *Journal of Geophysical Research*, 94, 1895-1912.

Eaton, D.W., Darbyshire, F., Evans, R.L., Grütter, H., Jones, A.G., & Yuan, X. (2009). The elusive lithosphere–asthenosphere boundary (LAB) beneath cratons. *Lithos*, 109, 1–22. https://doi.org/ 10.1016/j.lithos.2008.05.009

Emry, E.L., Shen, Y., Nyblade, A.A., Flinders, A., & Bao, X. (2018). Upper mantle Earth structure in Africa from full-wave ambient noise tomography. *Geochemistry, Geophysics, Geosystems*, 19. https://doi.org/10.1029/2018GC007804

Feeley, T.C. (2003). Origin and tectonic implications of across-strike geochemical variations in the Eocene Absaroka volcanic province, United States. *Journal of Geology*, 111, 329-346.

Feng, M., van der Lee, S., & Assumpção, M. (2007). Upper mantle structure of South America from joint inversion of waveforms and fundamental mode group velocities of Rayleigh waves. *Journal of Geophysical Research*, 112, B04312. https://doi.org/10.1029/2006JB004449

Fichtner, A., Bunge, H.-P., & Igel, H. (2006). The adjoint method in seismology – I. Theory. *Physics of the Earth and Planetary Interiors*, 157, 86-104.

Fichtner, A., Kennett, B. L. N., Igel, H., & Bunge, H.-P. (2009). Full seismic waveform tomography for upper-mantle structure in the Australasian region using adjoint methods. *Geophysical Journal International*, 179, 1703-1725.

Fichtner, A., van Herwaarden, D.-P., Afanasiev, M., Simute, S., Krischer, L., Cubuk-Sabuncu, Y., Taymaz, T., Colli, L., Saygin, E., Villasenor, A., Trampert, J., Cupillard, P., Bunge, H.-P., & Igel, H. (2018). The Collaborative Seismic Earth Model: Generation I. *Geophysical Research Letters,* 45, 4007-4016. https://doi.org/10.1029/2018GL077338

Fischer, K.M., Ford, H.A., Abt, D.L., & Rychert, C.A. (2010). The lithosphere – asthenosphere boundary. *Annual Reviews of Earth and Planetary Science*, 38, 551-575.

Fishwick, S., Kennett, B.L.N., & Reading, A.M. (2005). Contrasts in lithospheric structure within the Australian craton – insights from surface wave tomography. *Earth and Planetary Science Letters*, 231, 163-176. https://doi.org/10.1016/j.epsl.2005.01.009.

Foley, S.F. (2008). Rejuvenation and erosion of the cratonic lithosphere. *Nature Geoscience*, 1, 503-510.

Foster, D.A., Mueller, P.A., Mogk, D.W., Wooden, J.L., & Vogl, J.J. (2006). Proterozoic evolution of the western margin of the Wyoming craton: implications for the tectonic and magmatic evolution of the northern Rocky Mountains. *Canadian Journal of Earth Sciences*, 43, 1601-1619.

Frost, B.R., & Frost, C.D. (2019). *Essentials of Igneous and Metamorphic Petrology (2nd Ed.)*. Cambridge, UK: Cambridge University Press.

Frost, C.D., Frost, B.R., Chamberlain, K.R., & Hulsebosch, T.P. (1998). The Late Archean history of the Wyoming province as recorded by granite plutonism in the Wind River Range, Wyoming. *Precambrian Research*, 89, 145-173.

Frost, C.D., Fruchey, B.L., Chamberlain, K.R., & Frost, B.R. (2006). Archean crustal growth by lateral accretion of juvenile supracrustal belts in the south-central Wyoming province. *Canadian Journal of Earth Sciences*, 43, 1533-1555.

Frost, C. D., McLaughlin, J.F., Frost, B.R., Fanning, C.M., Swapp, S.M., Kruckenberg, S.C., & Gonzalez, J. (2017). Hadean origins of Paleoarchean continental crust in the central Wyoming Province. *Geological Society of America Bulletin*, 129, 259-280.

Gao, S., Rudnick, R.L., Carlson, R.W., McDonough, W.F., & Liu, Y.-S. (2002). Re–Os evidence for replacement of ancient mantle lithosphere beneath the North China craton. *Earth and Planetary Science Letters*, 198, 307–322.

Goleby, B.R., Blewett, R.S., Formin, T., Fishwick, S., Reading, A.M., Henson, P. A., Kennet, B.L.N., Champion, D.C., Jones, L., Drummon, B.J., & Nicoll, M. (2006). An integrated multi-scale 3D seismic model of the Archaean Yilgarn Craton, Australia. *Tectonophysics*, 420, 75-90. https://doi.org/10.1016/j.tecto.2006.01.028

Gorman, A. R., Clowes, R.M., Ellis, R.M., Henstock, T.J., Spence, G.D., Keller, G.R., Levander, A., Snelson, C.M., Burianyk, M.J.A., Kanasewich, E.R., Asudeh, I., Hajnal, Z., & Miller, K.C. (2002). Deep Probe: Imaging the roots of western North America. *Canadian Journal of Earth Sciences*, 39, 375–398. https://doi.org/10.1139/e01-064

Goutorbe, B., de Oliveira Coelho, D.L., & Drouet, S. (2015). Rayleigh wave group velocities at periods of 6-23 S across Brazil from ambient noise tomography. *Geophysical Journal International*, 203, 869-882.

Grand, S.P. (1994). Mantle shear structure beneath the Americas and surrounding oceans. *Journal of Geophysical Research*, 99, 11,591–11,621.

Griffin, W.L., O'Reilly, S.Y., Natapov, L.M., & Ryan, D.G. (2003). The evolution of lithospheric mantle beneath the Kalahari Craton and its margins. *Lithos*, 71, 215-242.

Griffin, W.L., Belousova, E.A., O'Neill, C., O'Reilly, S.Y., Valkovets, V., Pearson, N.J., Spetsius, S., & Wilde, S.A. (2014). The world turns over: Hadean-Archean crust-mantle evolution. *Lithos*, 189, 2-15. https://doi.org/10.1016/j.lithos.2013.08.018

Griffin, W. L., & O'Reilly, S. Y. (2007). Cratonic lithospheric mantle: is anything subducted? *Episodes*, 30, 43-53.

Hawkesworth, C.J., Cawood, P.A., Dhuime, B., & Kemp, T.I.S. (2017). Earth's continental lithosphere through time. *Annual Reviews of Earth and Planetary Science*, 45, 169-198.

Herzberg, C., & Rudnick, R. (2012). Formation of cratonic lithosphere: an integrated thermal and petrological model. *Lithos*, 149, 4-15.

Hopper, E., & Fischer, K.M. (2015). The meaning of midlithospheric discontinuities: a case study in the northern U.S. craton. *Geochemistry, Geophysics, Geosystems*, 16, 4057-4083.

Hu, J., Liu, L., Faccenda, M., Zhou, Q., Fischer, K.M., Marshak, S., & Lundstrom, C. (2018). Modification of the western Gondwana craton by plume-lithosphere interaction. *Nature Geoscience*, 11, 203-21. https://doi.org/10.1038/s41561-018-0064-1

Humphreys, E.D. (1995). Post-Laramide removal of the Farallon slab, western United States. *Geology*, 23, 987-990.

Jacobs, J., Pisarevsky, S., Thomas, R.J., & Becker T. (2008). The Kalahari Craton during the assembly and dispersal of Rodinia. *Precambrian Research*, 160, 142-158.

Jordan, T.H. (1975). The continental tectosphere. *Reviews of Geophysics and Space Physics*, 13, 1–12.

Jordan, T.H. (1979). Mineralogies, densities and seismic velocities of garnet lherzolites and their geophysical implications. In Boyd, F.R., and Meyer, H.O.A. (Eds.), *The Mantle Sample: Inclusions in Kimberlites and Other Volcanics: American Geophysical Union Special Publication* (Vol. 16, p. 1-14) Washington, DC: American Geophysical Union. https://doi.org/10.1029/SP16p0001

Jordan, T. H. (1988). Structure and formation of the continental tectosphere. *Journal of Petrology*, 1, 11–37.

Kamber, B.S. (2015). The evolving nature of terrestrial crust from the Hadean, through the Archaean, into the Proterozoic. *Precambrian Research*, 258, 48-82.

Karato, S.-I. (1995). Effects of water on seismic wave velocities in the upper mantle. *Proceedings of the Japan Academy, series B*, 71, 61–66.

Kemp, A.I.S., Wilde, S.A., Hawkesworth, C.J., Coath, C.D., Nemchin, A., Pidgeon, R.T., Vervoort, J.D., & Du-Frane, S.A. (2010). Hadean crustal evolution revisited: New constraints from Pb-Hf isotope systematics of the Jack Hills zircons. *Earth and Planetary Science Letters*, 296, 45–56. https://doi.org/10.1016/j.epsl.2010.04.043

Kennett, B.L.N., & Salmon, M. (2012). AuSREM: Australian Seismological Reference Model. *Australian Journal of Earth Sciences*, 59, 1091-1103. https://doi.org/10.1080/08120099.2012.736406

Kilian, T.M., Chamberlain, K.R., Evans, D.A.D., Bleeker, W., & Cousens, B.L. (2016). Wyoming on the run—toward final Paleoproterozoic assembly of Laurentia. *Geology*, 44, 863-866.

Kober, L. (1921). *Der Bau der Erde*. Berlin, Gebrüder Borntraeger. (Definition quoted is found on p. 21.)

Korenaga, J. (2008). Urey ratio and the structure and evolution of Earth's mantle. *Reviews of Geophysics*, 46, RG2007. https://doi.org/10.1029/2007RG000241

Kusky, T. M., Windley, B. F., Wang, L., Wang, Z., Li, X., & Zhu, P. (2014). Flat slab subduction, trench suction, and craton destruction: comparison of the North China, Wyoming, and Brazilian cratons. *Tectonophysics*, 3, 208–221.

Lee, C,-T.A. (2003). Compositional variation of density and seismic velocities in natural peridotites at STP conditions: implications for seismic imaging of compositional heterogeneities in the upper mantle. *Journal of Geophysical Research*, 108, 2441.

Lee, C.-T.A., Lenardic, A., Cooper, C.M., Niu, F., & Levander, A. (2005). The role of chemical boundary layers in regulating the thickness of continental and oceanic thermal boundary layers. *Earth and Planetary Science Letters*, 230, 379-395.

Lee, C.-T., Luffi, P., & Chin, E.J. (2011). Building and destroying continental mantle. *Annual Reviews of Earth and Planetary Sciences*, 39, 59-90. https://doi.org/10.1146/annurev-earth-040610-133505

Lei, J. (2012). Upper-mantle tomography and dynamics beneath the North China Craton. *Journal of Geophysical Research*, 117, B06313. https://doi.org/10.1029/2012JB009212

Lenardic, A., & Moresi, L.-N. (1999). Some thoughts on the stability of cratonic lithosphere: Effects of buoyancy and viscosity. *Journal of Geophysical Research: Solid Earth*, 104, 12,747–12,758. https://doi.org/10.1029/1999jb900035

Lenardic, A., Moresi, L., & Mühlhaus, H. (2000). The role of mobile belts for the longevity of deep cratonic lithosphere: the crumple zone model. *Geophysical Research Letters,* 27, 1235–1238.

Lenardic, A., Moresi, L.-N., & Mühlhaus, H. (2003). Longevity and stability of cratonic lithosphere: insights from numerical simulations of coupled mantle convection and continental tectonics. *Journal of Geophysical Research: Solid Earth*, 108, B6. https//doi.org/10.1029/2002JB001859

Li, B., Kung, J., & Liebermann, R.C. (2004). Modern techniques in measuring elasticity of Earth materials at high pressure and high temperature using ultrasonic interferometry in conjunction with synchrotron X-radiation in multi-anvil apparatus. *Physics of the Earth and Planetary Interiors,* 143, 559–574.

Liao, J., Wang, Q., Gerya, T., & Ballmer, M.D. (2017). Modeling craton destruction by hydration-induced weakening of the upper mantle. *Journal of Geophysical Research: Solid Earth*, 122, 7449-7466.

Liu, L., Morgan, J.P., Xu, Yiganag, & Menzies, M. (2018). Craton destruction 1: cratonic keel delamination along a weak midlithospheric discontinuity layer. *Journal of Geophysical Research: Solid Earth*, 123, 10,040-10,068. https://doi.org/10.1029/2017JB015372

Liu, L., Liu, L., Xu, Y.-G., Xia, B., Ma, Q., & Menzies, M. (2019). Development of a dense cratonic keel prior to the destruction of the north China craton: constraints from sedimentary records and numerical simulation. *Journal of Geophysical Research: Solid Earth*, 124, 13,192–13,206. https://doi.org/10.1029/2019JB018595

McCurry, M., Hayden, K.P., Morse, L.H., & Mertzman, S. (2008). Genesis of post-hotspot, A-type rhyolite of the Eastern Snake River Plain volcanic field by extreme fractional crystallization of olivine tholeiite. *Bulletin of Volcanology*, 70, 361-383.

McHone, J.G. (1996). Constraints on the mantle plume model for Mesozoic alkaline intrusions in northeastern North America. *Canadian Mineralogist*, 34, 325-334.

McKenzie, D., Daly, M. C., & Priestley, K. (2015). The lithospheric structure of Pangea. *Geology*, 43, 783–786. https://doi.org/10.1130/g36819.1

Menzies, M.A., Weiming, F,. & Zhang, M. (1993). Palaeozoic and Cenozoic lithoprobes and the loss of >120 km of Archaean lithosphere, Sino–Korean craton, China. In Prichard, H.M., Alabaster, T., Harris, N.B.W., and Neary, C.R., (Eds.), *Magmatic Processes and Plate*

Tectonics, Geological Society Special Publication, (Vol. 76, pp. 71–81). London: Geological Society.

Merdith, A.S., Williams, S.E., Brune, S., Collins, A.S., & Müller, R.D. (2019). Rift and plate boundary evolution across two supercontinent cycles. *Global and Planetary Change*, 173, 1-14.

Mole, D.R., Fiorentini, M.L., Thebaud, N., Cassidy, K.F., McCuaig, C.T., Kirkland, C.L., Romano, S.S., Doublier, M.P., Belousova, E.A., Barnes, S.J., & Miller, J. (2014). Archean komatiite volcanism controlled by the evolution of early continents. *Proceedings of the National Academy of Sciences*, 111, 10,083-10,0088.

Mueller, P.A., & Frost, C.D. (2006). The Wyoming province: a distinctive Archean craton in Laurentian North America. *Canadian Journal of Earth Sciences*, 43, 1391-1397.

Mueller, P. A., Wooden, J. L., Nutman, A. P., & Mogk, D. W. (1998). Early Archean crust in the northern Wyoming province - Evidence from U-Pb ages of detrital zircons. *Precambrian Research*, 91, 295-307.

Nebel, O., Rapp, R.P., & Yaxley, G.M., (2014). The role of detrital zircons in Hadean crustal research. *Lithos*, 190-191, 313-327. https://doi.org/10.1016/j.lithos.2013.12.010

Nyblade, A.A., & Pollack, H.N. (1993). A global analysis of heat flow from Precambrian terrains: implications for the thermal structure of Archean and Proterozoic lithosphere. *Journal of Geophysical Research*, 98, 12,207-12,218.

Oversby, V.M. (1975). Lead isotopic systematics and ages of Archaean acid intrusives in the Kalgoorlie-Norseman area, western Australia. *Geochimica et Cosmochimica Acta*, 39, 1107-1125.

Oxburgh, E.R., & Turcotte, D.L. (1971). Origin of paired metamorphic belts and crustal dilation in island arc regions. *Journal of Geophysical Research*, 76, 1315-1327.

Paul, J., Ghosh, A., & Conrad, C.P. (2019). Traction and strain-rate at the base of the lithosphere: an insight into cratonic survival. *Geophysical Journal International*, 217, 1024-1033.

Petersson, A., Kemp, A.I.S., & Whitehouse, M. (2019). A Yilgarn seed to the Pilbara Craton (Australia)? Evidence from inherited zircons. *Geology*, 47, 1098-1102.

Polat, A., Herzberg, C., Munker, C., Rodgers, R., Kusky, T., Li, J., Fryer, B., & Delaney, J. (2006). Geochemical and petrological evidence for a suprasubduction zone origin of

Neoarchean (ca. 2.5 Ga) peridotites, central orogenic belt, North China craton. *Geological Society of America Bulletin*, 118, 771-784.

Pollack, H.N. (1986). Cratonization and thermal evolution of the mantle. *Earth and Planetary Science Letters*, 80, 175-182. https://doi.org/10.1016/0012-821X(86)90031-2

Porritt, R. W., Allen, R. M. & Pollitz, F. F. (2014). Seismic imaging east of the Rocky Mountains with USArray. *Earth and Planetary Science Letters*, 402, 16-25. https://doi:10.1016/j.epsl.2013.10.034

Portner, D. E., Rodríguez, E. E., Beck, S., Zandt, G., Scire, A., Rocha, M. P., Bianchi, M.B., Ruiz, M., Franca, G.S., Condori, C., & Alvarado, P. (2020). Detailed structure of the subducted Nazca slab into the lower mantle derived from continent-scale teleseismic P wave tomography. *Journal of Geophysical Research: Solid Earth*, 125, e2019JB017884.

Poudjom Djomani, Y.H., O'Reilly, S.Y., Griffin, W.L., & Morgan, P. (2001). The density structure of subcontinental lithosphere through time. *Earth and Planetary Science Letters*, 184, 605-621.

Priestley, K., McKenzie, D., & Ho, T. (2019). A Lithosphere–Asthenosphere Boundary—a Global Model Derived from Multimode Surface-Wave Tomography and Petrology. In Yuan, H., and Romanowicz, B. (Eds.), *Lithospheric Discontinuities, Geophysical Monograph Series* (Vol. 239, pp. 111-123). Washington, DC. American Geophysical Union. https://doi.org/10.1002/9781119249740.ch6.

Prodehl, C., & Mooney, W.D. (2012). Exploring the Earth's crust — history and results of controlled-source seismology. *Geological Society of America Memoir* (Vol. 208, 784 p.)

Rajesh, H.M., Chisonga, B.C., Shindo, K., Beukes, N.J., & Armstrong, R.A. (2013). Petrographic, geochemical and SHRIMP U-Pb titanite age characterization of the Thabazimbi mafic sills: extended time frame and a unifying petrogenetic model for the Bushveld Large Igneous Province. *Precambrian Research*, 230, 79-102.

Rasmussen, R., Fletcher, I.R., Muhling, J.R., & Wilde, S.A. (2010). In situ U-Th–Pb geochronology of monazite and xenotime from the Jack Hills belt: Implications for the age of deposition and metamorphism of Hadean zircons. *Precambrian Research*, 180, 26-46.

Reeves, C. (2014). The position of Madagascar within Gondwana and its movements during Gondwana dispersal. *Journal of African Earth Sciences*, 94, 45-57.

Richardson, S.H., & Shirey, S.B. (2008). Continental mantle signature of Bushveld magmas and coeval diamonds. *Nature*, 453, 910-913.

Sandu, C., Lenardic, A., O'Neill, C.J., & Cooper, C.M. (2011). Earth's evolving stress state and the past, present, and future stability of cratonic lithosphere. *International Geology Review*, 53, 1392-1402.

Santos, J.O.S., Rizzotto, G.J., Potter, P.E., McNaughton, N.J., Matos, R.S., Hartmann, L.A., Chemale, F. & Quadros, M.E.S. (2008). Age and autochthonous evolution of the Sunsas Orogen in West Amazon Craton based on mapping and U-Pb geochronology. *Precambrian Research*, 165, 120–152.

Saygin, E., & Kennett, B. (2019). Retrieval of interstation local body waves from teleseismic coda correlations. *Journal of Geophysical Research: Solid Earth*, 124, 2957-2969.

Schmandt, B., & Humphreys, E. (2010). Complex subduction and small-scale convection revealed by body-wave tomography of the western United States upper mantle. *Earth and Planetary Science Letters*, 297, 435-445.

Schmitz, M. D., Bowring, S. A., de Wit, M. J. & Gartz, V. (2004). Subduction and terrane collision stabilized the western Kaapvaal craton tectosphere 2.9 billion years ago. *Earth and Planetary Science Letters*, 222, 363–376.

Scotese, C.R., & Elling, R. (2017). Plate Tectonic Evolution during the Last 1.5 Billion Years: The Movie. *Plate Tectonics at 50, William Smith Meeting*, October 3-5, 2017, The Geological Society, Burlington House, London, p. 16-17, https://blog.geolsoc.org.uk/2017/12/01/door-1-1-5-billion-years-of-plate-tectonic-stories/.

Selway, K., Ford, H., & Keleman, P.B. (2015). The seismic mid-lithosphere discontinuity. *Earth and Planetary Science Letters*, 414, 45-57.

Şengör, A.M.C. (1999). Continental interiors and cratons: any relation? *Tectonophysics*, 305, 1-42.

Sheppard, S., Krapez, B., Zi, J.-W., Rasmussen, B., & Fletcher, I. (2017). SHRIMP U-Pb geochronology establishes that banded iron formations are not chronostratigraphic markers across Archean greenstone belts of the Pilbara Craton. *Precambrian Research*, 292, 290-304.

Shirey, S.B., Harris, J.W., Richardson, S.H., Fouch, M., James, D.E., Cartigny, P., Deines, P., & Viljoen, F. (2003). Regional patterns in the paragenesis and age of inclusions in diamond,

diamond composition, and the lithospheric seismic structure of southern Africa. *Lithos,* 71, 243-258.

Silva-Silva, L.C., Oliveira, D.C., & Barbosa de Souza, D. (2020). Geology and geochemical constraints on the origin of the Mesoarchean granitoids from Carajas province, Amazonian craton. *Journal of South American Earth Sciences*, 100, 102568.

Simon, N.S., Carlson, R.W., Pearson, D.G., & Davies, G.R. (2007). The origin and evolution of the Kaapvaal cratonic lithospheric mantle. *Journal of Petrology*, 48, 589-625.

Sleep, N. H. (2005). Evolution of the continental lithosphere. *Annual Review of Earth and Planetary Sciences,* 33, 369–393. https://doi.org/10.1146/annurev.earth.33.092203.122643

Snelson, C.M., Henstock, T.J. Keller, G.R. Miller, K.C. & Levander, A. (1998). Crustal and uppermost mantle structure along the Deep Probe seismic profile. *Rocky Mountain Geology*, 33, 181–198.

Snyder, D.B., Humphreys, E., & Pearson, D.G. (2017). Construction and destruction of some North American cratons. *Tectonophysics*, 694, 464-485.

Stille, H. (1940). *Einführung in den Bau Amerikas*. Berlin, Gebrüder Borntraeger, 717 p. (Quotation appears on p. 655.)

Tao, K., Grand, S., & Niu, F. (2018). Seismic Structure of the Upper Mantle Beneath Eastern Asia From Full Waveform Seismic Tomography. *Geochemistry, Geophysics, Geosystems*. https://doi:19.10.1029/2018GC007460.

Taylor, P.N., Kramers, J.S., Moorbath, S., Wilson, J.F., Orpen, J.L., et al. (1991). Pb/Pb, Sm-Nd and Rb-Sr geochronology in the Archean craton of Zimbabwe. *Chemical Geology; Isotope Geoscience Section,* 87, 175-196.

Tian, Y., Zhao, D., Sun, R., & Teng, J. (2009). Seismic imaging of the crust and upper mantle beneath the North China Craton. *Physics of the Earth and Planetary Interiors*, 172, 169–182.

Trabant, C., Hutko, A.R., Bahavar, M., Karstens, R., Ahern, T., & Aster, R. (2012). Data Products at the IRIS DMC: Stepping Stones for Research and Other Applications. *Seismological Research Letters*, 83, 846–854. https://doi.org/10.1785/0220120032

Tucker, R.D., Roig, J.Y., Delor, C., & Peters, S.G. (2014). A geological synthesis of the Precambrian shield in Madagascar. *Journal of African Earth Sciences*, 94, 9-30.

Turcotte, D. L., & Schubert, G. (2002). *Geodynamics*. Cambridge, Cambridge University Press, 636 p.

Van Kranendonk, M.J., Ivanic, T.J., Wingate, M.T.D., Kirkland, C.L., & Wyche, S. (2013). Long-lived, autochthonous development of the Archean Murchison Domain and implications for Yilgarn Craton tectonics. *Precambrian Research*, 229, 49-92.

Van Kranendonk, M.J., Smithies, R.H., Griffin, W.L., Huston, D.L., Hickman, A.H., Champion, D.C., Anhaeusser, C.R., & Pirajno, F. (2015). Making it thick: a volcanic plateau origin of Palaeoarchean continental lithosphere of the Pilbara and Kaapvaal cratons. In Roberts, N.M.W., Van Kranendonk, M., Parman, S., Shirey, S., & Clift, P.D. (Eds.), *Continent Formation Through Time*, Geological Society Special Publications (Vol. 389, pp. 83-111). London: Geological Society of London.

Van Kranendonk, M.J., Smithies, R.H., & Champion, D.C. (2019). Paleoarchean development of a continental nucleus: the East Pilbara Terrane of the Pilbara Craton, Western Australia. In Van Kranendonk, M.J., Bennett, V.C., and Hoffmann, J.E. (Eds.), *Earth's Oldest Rocks, 2nd Edition*, (pp. 437-462). Amsterdam, Elsevier.

Wall, C.J., Scoates, J.S., Weis, D., Friedman, R.M., Amini, M., & Meurer, W.P. (2018). The Stillwater complex: integrating zircon geochronological and geochemical constraints on the age, emplacement history and crystallization of a large, open-system layered intrusion. *Journal of Petrology*, 59, 153-190.

Wan, Y., Wu., J., Liu, D., Chang, Z., & Biao, S. (1997). Geochemistry and Nd, Pb isotopic characteristics of 3.3 Ga Chentaigou granite in Anshan area. *Acta Geoscientia Sinica*, 18, 382-388.

Wan, Y., Xie, H., Dong, C., Kroner, A., Wilde, S.A., Bai, W., Liu, S., Xie, S., Ma, M., Li, Y., & Liu, D. (2019). Hadean to Paleoarchean rocks and zircons in China. In Van Kranendonk, M.J., Bennett, V.C., & Hoffmann, J.E. (Eds.), *Earth's Oldest Rocks, 2nd Edition* (pp. 293-327). Amsterdam, Elsevier.

Wang, X., Zhu, P., Kusky, T.M., Zhao, N., Li, X., & Wang, Z. (2016). Dynamic cause of marginal lithospheric thinning and implications for craton destruction: a comparison of the North China, Superior, and Yilgarn cratons. *Canadian Journal of Earth Sciences*, 53, 1121-1141.

Wang, H., van Hunen, J., Pearson, D. G., & Allen, M. B. (2014). Craton stability and longevity: The roles of composition-dependent rheology and buoyancy. *Earth and Planetary Science Letters,* 391, 224–233.

Wenker, S., & Beaumont, C. (2018a). Effects of lateral strength contrasts and inherited heterogeneities on necking and rifting of continents. *Tectonophysics,* 746, 46-63.

Wenker, S., & Beaumont, C. (2018b). Can metasomatic weakening result in the rifting of cratons? *Tectonophysics*, 746, 3-21.

Wooden, J.L., & Mueller, P.A. (1988). Pb, Sr, and Nd isotopic compositions of a suite of Late Archean, igneous rocks, eastern Beartooth Mountains: implications for crust-mantle evolution. *Earth and Planetary Science Letters*, 87, 59-72.

Wu, F. Y., Yang, J. H., Xu, Y. G., Wilde, S. A., & Walker, R. J. (2019). Destruction of the North China craton in the Mesozoic. *Annual Review of Earth and Planetary Sciences*, 47, 173-195.

Xu, C., Kynicky, J., Song, W., Tao, R., Lu, Z., Li, Y., Yang, Y., Pohanka, M., Galiova, M.B., Zhang, L., & Fei, Y.. (2018). Cold deep subduction recorded by remnants of a Paleoproterozoic carbonated slab. *Nature Communications*, 9, 2790. https://doi.org/10.1038/s41467-018-05140-5.

Yoshida, M. (2010). Preliminary three-dimensional model of mantle convection with deformable, mobile continental lithosphere. *Earth and Planetary Science Letters*, 295, 205-218.

Yoshida, M. (2012). Dynamic role of the rheological contrast between cratonic and oceanic lithospheres in the longevity of cratonic lithosphere: A three-dimensional numerical study. *Tectonophysics*, 532, 156-166.

Yousef, M., Thybo, H. Artemieva, I.M. & Levander, A. (2015). Upper mantle structure beneath southern African cratons from seismic finite-frequency P- and S-body wave tomography. *Earth and Planetary Science Letters*, 420, 174-186.

Yuan, H., & Dueker, K. (2005). Upper mantle tomographic Vp and Vs images of the Rocky Mountains in Wyoming, Colorado and New Mexico: Evidence for a thick heterogeneous chemical lithosphere. In Keller, G. R. and Kalstrom, K. E. (Eds.), *The Rocky Mountain Region: An Evolving Lithosphere: Tectonics, Geochemistry, and Geophysics*.

Geophysical Monograph Series (Vol. 154, pp. 329-345). Washington, DC: American Geophysical Union. https://doi.org/10.1029/154GM25.

Zeh, A., Gerdes, A., & Barton, J.M. (2009). Archean accretion and crustal evolution of the Kalahari Craton—the zircon age and Hf isotope record of granitic rocks from Barberton/Swaziland to the Francistown Arc. *Journal of Petrology*, 50, 933-966. https://doi.org/10.1093/petrology/egp027.

Zhao, G., Sun, M., Wilde, S.A., & Sanzhong, L. (2005). Late Archean to Paleoproterozoic evolution of the North China Craton: key issues revisited. *Precambrian Research*, 136, 177-202.

Zhang, S., Li, Z.-X., Evans, D.A.D., Wu, H., Li, H., & Dong, J. (2012). Pre-Rodinia supercontinent Nuna shaping up: a global synthesis with new paleomagnetic results from North China. *Earth and Planetary Science Letters*, 353-354, 145-155.

Zheng, J., Griffin, W.L., O'Reilly, S.Y., Liou, J.G., Zhang, R.Y., & Lu, F. (2005). Late Mesozoic-Eocene mantle replacement beneath the eastern North China Craton: evidence from the Paleozoic and Cenozoic peridotite xenoliths. *International Geology Review*, 47, 457-472. https://doi.org/10.2747/0020-6814.47.5.457

Zheng, Y., Shen, W., Zhou, L., Yang, Y., Xie, Z., & Ritzwoller, M. H. (2011). Crust and uppermost mantle beneath the North China Craton, northeastern China, and the Sea of Japan from ambient noise tomography. *Journal of Geophysical Research*, 116, B12312, https://doi.org/10.1029/2011JB008637